

1 **A functional taxonomy of tumor suppression in oncogenic KRAS-driven lung cancer**

2
3 Hongchen Cai^{1*}, Su Kit Chew^{5*}, Chuan Li^{4*}, Min K. Tsai¹, Laura Andrejka¹, Christopher W. Murray²,
4 Nicholas W. Hughes¹, Emily G. Shuldiner⁴, Emily L. Ashkin², Rui Tang¹, King L. Hung², Leo C. Chen¹,
5 Shi Ya C. Lee⁵, Maryam Yousefi¹, Wen-Yang Lin¹, Christian A. Kunder³, Le Cong^{1,3}, Christopher D.
6 McFarland⁴, Dmitri A. Petrov^{2,4#}, Charles Swanton^{5,6#}, Monte M. Winslow^{1,2,3#}

7
8 ¹ Department of Genetics, Stanford University School of Medicine, Stanford, CA, USA

9 ² Cancer Biology Program, Stanford University School of Medicine, Stanford, CA, USA

10 ³ Department of Pathology, Stanford University School of Medicine, Stanford, CA, USA

11 ⁴ Department of Biology, Stanford University, Stanford, CA, USA

12 ⁵ Cancer Evolution and Genome Instability Laboratory, University College London Cancer Institute, London, UK.

13 ⁶ Cancer Evolution and Genome Instability Laboratory, The Francis Crick Institute, London, UK.

14 * These authors contributed equally

15 # Corresponding authors:

16 Monte M. Winslow, Stanford University School of Medicine | 279 Campus Drive, Beckman Center B256, Stanford, CA 94305.

17 Phone: 650-725-8696 | Fax: 650-725-1534 | E-mail: mwWinslow@stanford.edu

18

19 Charles Swanton, Cancer Evolution and Genome Instability Laboratory, The Francis Crick Institute, 1 Midland Road,
20 London, NW1 1AT, United Kingdom. Phone: +44 203 796 2047 | Email: Charles.Swanton@crick.ac.uk

21

22 Dmitri A. Petrov, Biology Department, Stanford University, Bass Biology Building, 327 Campus Drive Stanford 94305. Phone:
23 650-736-1169| Fax: 650-7366132 | E-mail: dpetrov@stanford.edu

24

25 **RUNNING TITLE**

27 A functional taxonomy of tumor suppression in lung cancer

28

29 **CONFLICT OF INTERESTS**

30 S.K.C. receives grant support from Ono Pharma. C.S. acknowledges grant support from
31 Pfizer, AstraZeneca, Bristol Myers Squibb, Roche-Ventana, Boehringer-Ingelheim, Archer Dx Inc
32 (collaboration in minimal residual disease sequencing technologies) and Ono Pharmaceuticals. C.S
33 is an AstraZeneca Advisory Board member and Chief Investigator for the MeRmaiD1 clinical trial,
34 has consulted for Pfizer, Novartis, GlaxoSmithKline, MSD, Bristol Myers Squibb, Celgene,

35 AstraZeneca, Illumina, Amgen, Genentech, Roche-Ventana, GRAIL, Medicxi, Bicycle
36 Therapeutics, and the Sarah Cannon Research Institute, has stock options in Apogen
37 Biotechnologies, Epic Bioscience, GRAIL, and has stock options and is co-founder of Achilles
38 Therapeutics. D.A.P. and M.M.W. are founders of, and hold equity in, D2G Oncology Inc.

39

40 **ABSTRACT**

41 Cancer genotyping has identified a large number of putative tumor suppressor genes.
42 Carcinogenesis is a multi-step process, however the importance and specific roles of many of
43 these genes during tumor initiation, growth and progression remain unknown. Here we use a
44 multiplexed mouse model of oncogenic KRAS-driven lung cancer to quantify the impact of
45 forty-eight known and putative tumor suppressor genes on diverse aspects of carcinogenesis at
46 an unprecedented scale and resolution. We uncover many previously understudied functional
47 tumor suppressors that constrain cancer *in vivo*. Inactivation of some genes substantially
48 increased growth, while the inactivation of others increases tumor initiation and/or the
49 emergence of exceptionally large tumors. These functional *in vivo* analyses revealed an
50 unexpectedly complex landscape of tumor suppression that has implications for understanding
51 cancer evolution, interpreting clinical cancer genome sequencing data, and directing approaches
52 to limit tumor initiation and progression.

53

54 **STATEMENT OF SIGNIFICANCE**

55 Our high-throughput and high-resolution analysis of tumor suppression uncovered novel
56 genetic determinants of oncogenic KRAS-driven lung cancer initiation, overall growth, and
57 exceptional growth. This taxonomy is consistent with changing constraints during the life history
58 of cancer and highlights the value of quantitative *in vivo* genetic analyses in autochthonous
59 cancer models.

60

61

62

63 **INTRODUCTION**

64 Cancer initiation and development is a multi-step process driven in large part by cancer
65 cell-intrinsic alterations (1). Over the past several decades, cancer genome sequencing has
66 contributed to our understanding of the genetic drivers of cancer and identified a large number of
67 putative tumor suppressor genes (2-8). However, genome sequencing data is insufficient to
68 determine the importance of these genes during various stages of carcinogenesis (9). The nature
69 and frequency of genomic alterations also provide limited insight into the modes of action of
70 putative tumor suppressor genes, underscoring the importance of functional genomics in
71 elucidating gene function (10,11).

72 Tumor suppressors regulate many different pathways and cellular processes. Assessing
73 their impact on tumor initiation and each step of cancer development not only distinguishes
74 driver from passenger genes but also highlights different pathways and processes that constrain
75 carcinogenesis across the course of the disease (12,13). Thus, *in vivo* functional genomic
76 approaches are critical for understanding cancer evolution (14-16), interpreting clinical cancer
77 genome sequencing data (17,18), and directing precision medicine approaches (19,20).

78 *In vivo* cancer models in which tumor initiation and growth occurs entirely within the
79 autochthonous environment are uniquely tractable systems to uncover gene function (21). The
80 integration of CRISPR/Cas9 somatic genome editing into genetically engineered mouse models
81 of human cancer has facilitated the rapid analysis of gene function *in vivo* (22-25). Recently, the
82 combination of somatic CRISPR-based genome editing with tumor barcoding and high-
83 throughput barcode sequencing (Tuba-seq) has greatly increased the scale and precision of these
84 *in vivo* approaches (26,27). These types of approaches can quantify the impact of many
85 engineered genomic alterations on cancer growth *in vivo* in a multiplexed manner (12,26-28).

86 Here we integrate multiple critical advances in our Tuba-seq pipeline and quantify the
87 roles of a broad range of diverse putative tumor suppressors across multiple facets of
88 carcinogenesis. By uncovering the extent to which different tumor suppressors govern tumor
89 initiation, growth and acquisition of altered phenotypes across time, we uncover an unexpectedly
90 complex taxonomy of tumor suppression across the life history of oncogenic KRAS-driven lung
91 cancer.

92

93 RESULTS

94 Prioritization of candidate tumor suppressor genes

95 To characterize the functional landscape of tumor suppression, we selected 48 known and
96 putative tumor suppressor genes to investigate using Tuba-seq in a model of oncogenic KRAS-
97 driven lung cancer (**Fig. 1A; Methods**). These genes were chosen based on multiple criteria
98 including their mutational frequency in lung adenocarcinoma from TCGA, GENIE, and
99 TRACERx datasets, their mutational frequency in pan-cancer genomic data, and the consistency
100 of their mutational profiles with tumor suppressor activity (**Fig. 1A and B; Supplementary Fig.**
101 **S1A-E and Table S1**(2,4-7). We also considered their putative tumor-suppressive function in
102 other cancer types as well as their molecular functions (**Supplementary Fig. S2A and**
103 **B**)(8,29,30). Our candidate genes vary greatly in their mutation frequency and co-occurrence
104 with oncogenic KRAS alterations (**Supplementary Fig. S1C-E**). Importantly, these genes
105 include well-studied tumor suppressors as well as genes for which there is very limited evidence
106 supporting a role in constraining any aspect of carcinogenesis (**Supplementary Fig. S3A and B**).
107

108 **Quantitative analysis uncovers diverse tumor suppressors with distinct abilities to**
109 **constrain tumor growth *in vivo***

110 To determine the impact of inactivating each candidate tumor suppressor gene on
111 carcinogenesis *in vivo*, we used Tuba-seq to quantify the tumor size profiles after inactivation of
112 each gene (**Supplementary Fig. S4A**). We generated at least two Lenti-sgRNA/Cre vectors with
113 distinct sgRNAs targeting each gene and five Lenti-sgInert/Cre negative control vectors (102
114 total vectors; **Fig. 1C; Supplementary Table S2**). Each vector contains a two-component sgID-
115 BC, where the sgID uniquely identifies the sgRNA and the diverse random 20-nucleotide
116 barcode (BC) uniquely labels each clonal tumor. We generated each lentiviral vector separately
117 and pooled them to generate a highly multiplexed vector pool (Lenti-sgTS102/Cre; **Fig. 1C**;
118 **Methods**). We initiated lung tumors with this pool in *Kras*^{LSL-G12D/+}; *R26*^{LSL-Tom}; *H11*^{LSL-Cas9}
119 (*KT*; *H11*^{LSL-Cas9}) mice and Cas9-negative control *Kras*^{LSL-G12D/+}; *R26*^{LSL-Tom} (*KT*) mice. These
120 Cas9-negative mice are necessary to confirm that all vectors have little impact on tumor growth
121 in the absence of Cas9 and to calculate genotype-specific effects on tumor number (see below).
122 Fifteen weeks after tumor initiation, *KT*; *H11*^{LSL-Cas9} mice had visibly larger tumors than *KT* mice
123 (**Fig. 1D**). We extracted DNA from bulk tumor-bearing lungs and used Tuba-seq to quantify
124 overall tumor burden and the sizes of each tumor, of each genotype, in each mouse.

125 *KT*; *H11*^{LSL-Cas9} mice had ~10-fold higher total neoplastic cell number and proportionally
126 increased total lung weight (**Fig. 1E**). Initial analysis of the impact of each sgRNA on tumor
127 burden (a metric of the relative number of neoplastic cells in all tumors of the same sgRNA)
128 highlighted many genes as functional tumor suppressors. Even this relatively crude metric, which
129 does not incorporate the per-tumor resolution of Tuba-seq, uncovered genes where both sgRNAs
130 increased tumor burden (**Fig. 1F**). To investigate which aspects of carcinogenesis are regulated

131 by putative tumor suppressor genes, we calculated multiple summary statistics. We applied our
132 experimental design to identify tumor suppressor genes that normally limit overall tumor growth,
133 tumor initiation, and the emergence of exceptionally large tumors (**Fig. 1C; Supplementary Fig.**
134 **S4B, S4C; Methods**).

135

136 **Many diverse tumor suppressor genes increased overall tumor growth**

137 The ability of Tuba-seq to quantify the number of neoplastic cells in thousands of tumors
138 of each genotype allowed us to precisely assess their impact on tumor growth with greater
139 precision than previous approaches. We calculated two metrics of tumor growth from the
140 distribution of tumor sizes to uncover the effect of inactivating each tumor suppressor on overall
141 tumor growth (tumor sizes at defined percentiles within the tumor size distribution and log-
142 normal mean, **Methods; Supplementary Fig. S4B**). As expected, tumors initiated with each
143 Lenti-sgRNA/Cre vector in control Cas9-negative *KT* mice had very similar tumor size profiles,
144 suggesting that our pipeline is free from bias and false-positive signals (**Supplementary Fig.**
145 **S5A**). Consistent with previous Cre/lox and CRISPR/Cas9-based mouse models (22,26,31-34),
146 inactivation of *Stk11/Lkb1*, *Pten*, *Setd2*, and *Nfl* in tumors in *KT;H11^{LSL-Cas9}* mice greatly
147 increased tumor growth (**Fig. 2A-C; Supplementary Fig. S5B**). Importantly, inactivation of
148 STAG2, a cohesin complex component, increased tumor growth to a comparable extent as
149 inactivation of those well-established tumor suppressors (**Fig. 2A-C; Supplementary Fig. S5B**).

150 Inactivation of 14 other genes, including *Cdkn2c*, *Cmtr2*, *Rb1*, *Rnf43*, *Tsc1*, and *Rbm10*,
151 significantly increased tumor growth (**Fig. 2A-C; Supplementary Fig. S5**). These 14 genes
152 include not only well-established tumor suppressors such as *Rb1* and *Cdkn2a*, but also many
153 genes that have not been previously considered functional tumor suppressors in lung

154 adenocarcinoma or cancer in general. For example, the effects of inactivating *Cmtr2* and *Rnf43*
155 were particularly dramatic and unexpected (**Fig. 2B**). CMTR2 is the sole cap2 2'-O-ribose
156 methylase that modifies the 5'-cap of mRNAs and small nuclear RNAs and is mutated in ~2.2%
157 of lung adenocarcinomas and 1.4% of all cancers (7,35)(**Supplementary Table S1**). No previous
158 studies have investigated its function in cancer, and no commercial or academic cancer gene
159 sequencing panels include *CMTR2* (**Supplementary Fig. S3A and B**). RNF43 is a
160 transmembrane E3 ubiquitin ligase that targets Wnt receptors for lysosomal degradation (36).
161 *RNF43* is frequently mutated across multiple cancer types, including in colorectal and pancreatic
162 adenocarcinoma, where *RNF43* deficiency has been shown to sensitize cancer cells to porcupine
163 inhibitors (37,38). Thus, our broad survey pinpointed multiple novel functional tumor
164 suppressors in oncogenic KRAS-driven lung cancer and revealed commonality among cancer
165 subtypes.

166

167 **STAG2 is a novel functional tumor suppressor**

168 From our initial analysis of overall tumor growth suppression, STAG2 emerged as a
169 particularly interesting and novel suppressor of lung tumor growth. *STAG2* is mutated in ~4% of
170 lung adenocarcinomas and cohesin complex components are altered in ~10% of lung
171 adenocarcinomas (**Supplementary Fig. S6A, S6B and Table S1**). STAG2 has been implicated
172 as a tumor suppressor in bladder cancer, regulates lineage-specific genes in acute myeloid
173 leukemia, and is mutated across diverse cancer types (39-42). However, no previous studies have
174 suggested STAG2 as a critical suppressor of lung cancer growth. To further investigate the
175 tumor-suppressive effect of STAG2, we initiated lung tumors in *KT* and *KT;H11^{LSL-Cas9}* mice
176 with individual Lenti-sgInert/Cre and Lenti-sgStag2/Cre vectors (**Supplementary Fig. S7A**).

177 Relative to control cohorts, *Stag2* inactivation dramatically increased tumor burden
178 (**Supplementary Fig. S7B-E**). Inactivation of *Stag2* in lung tumors in *KT;H11^{LSL-Cas9}* mice also
179 significantly reduced long-term survival, consistent with its tumor growth-suppressive function
180 (**Supplementary Fig. S7F**).

181 To further characterize STAG2-mediated lung tumor growth suppression, we assessed
182 tumor growth in *KT* mice with Cre/lox-mediated inactivation of *Stag2* (**Fig. 3A**). *Stag2* is
183 located on the X-chromosome, thus both heterozygous and homozygous *Stag2* deletion in female
184 mice and hemizygous *Stag2* deletion in male mice generated tumors that lacked STAG2 protein
185 (**Fig. 3B and C**). *Stag2* inactivation dramatically increased lung tumor burden, and mice with
186 *Stag2*-deficient tumors had markedly shorter overall survival (**Fig. 3D-G**). *Stag2*-deficient and
187 proficient lung tumors were atypical adenomatous hyperplasias, adenomas, and early
188 adenocarcinomas that were uniformly NKX2-1/TTF1-positive. Interestingly, some *Stag2*-
189 deficient tumors had nuclear palisading and were histologically distinct from the tumors that
190 developed in control *KT* mice (**Supplementary Fig. S7G-I**). STAG2 inactivation in other
191 cancer- and cell-types is associated with chromosomal instability (43,44), increased DNA
192 damage (45,46), and activation of MEK/ERK or cGAS/STING signaling (47,48). However,
193 immunohistochemistry and analysis of canonical target genes suggest that these mechanisms are
194 unlikely to be major drivers of the increased growth in *Stag2*-deficient lung cancer
195 (**Supplementary Fig. S8A-E**). Thus, further work will be necessary to determine the molecular
196 mechanisms of tumor suppression driven by STAG2.

197 Finally, to further characterize the expression of STAG2 in lung cancer, we perform
198 immunohistochemistry for STAG2 on 479 human lung adenocarcinomas. About 20% of tumors
199 were low or negative for STAG2 protein, suggesting that an even larger fraction of lung

200 adenocarcinomas may be driven by alterations in this pathway (**Fig. 3H**). Interestingly, STAG2-
201 low/negative tumors were often more poorly differentiated and advanced human lung
202 adenocarcinomas (**Fig. 3I**).
203

204 **Additional tumor-suppressive effects emerge at later time points**

205 To gain further insights into the dynamics of tumor suppression in lung cancer, we
206 assessed tumor suppressor gene function at a later timepoint after tumor initiation. We reasoned
207 that allowing tumors to grow for a longer period of time might uncover greater magnitudes of
208 growth-suppression for genes that initially had modest effects and could highlight additional
209 tumor suppressors that play more important roles only at later stages of tumor growth. To allow
210 mice to survive for a longer period of time after tumor initiation, we generated a second pool of
211 Lenti-sgRNA/Cre vectors, which excluded those targeting *Lkb1*, *Pten*, *Setd2*, *Nfl*, *p53*, *Stag2*,
212 *Cdkn2c* and *Rb1* that collectively accounted for more than half of the total tumor burden (Lenti-
213 sgTS85/Cre; **Fig. 4A**). We initiated tumors in *KT;H11^{LSL-Cas9}* mice with a titer of Lenti-
214 sgTS85/Cre that would allow them to survive for 26 weeks while maximizing tumor number to
215 achieve reasonable statistical power (**Fig. 4A; Supplementary Fig. S9A; Methods**). As
216 controls, we also initiated tumors with Lenti-sgTS85/Cre pool in *KT;H11^{LSL-Cas9}* and *KT* mice
217 and analyzed them after 15 weeks (**Fig. 4A**).

218 After 26 weeks of tumor growth, inactivation of *Cdkn2a*, *Dnmt3a*, *Cmtr2*, *Kdm6a* and
219 *Ncoa6* significantly increased tumor burden (**Fig. 4B**). Furthermore, inactivation of *Rbm10*,
220 *Cmtr2*, *Rnf43* and *Tsc1* also still increased tumor sizes at defined percentiles of the distribution
221 as well as the log-normal mean tumor size at this later time point (**Supplementary Fig. S9B**).
222 These results confirm the tumor-suppressive function of these genes. Importantly, inactivation of

223 several other genes that had marginal to no effects on tumor sizes after 15 weeks of tumor
224 growth, including *Keap1*, *Kdm6a*, *Ncoa6*, *Cdkn2a*, *Dnmt3a* and *Dot1l*, broadly increased tumor
225 sizes after 26-weeks of tumor growth (**Fig. 4C-F**). Thus, analysis of growth metrics at multiple
226 time points after tumor initiation can provide temporal resolution of tumor suppressor gene
227 effects.

228

229 **Tuba-seq captures additional aspects of tumor suppressor gene function**

230 In addition to uncovering tumor suppressor genes that limit overall growth, our methods
231 can quantify other aspects of cancer initiation and progression impacted by these genes and
232 pathways. The relative tumor burden induced by each Lenti-sgRNA/Cre vector was mostly
233 consistent with the growth effects uncovered using tumor sizes at defined percentiles
234 (**Supplementary Fig. S10A**). However, the effects of inactivating some genes on relative tumor
235 burden were disproportionately large (**Supplementary Fig. S10A and B**). For example, *p53* was
236 clearly a tumor suppressor based on relative tumor burden but *p53* inactivation did not greatly
237 increase overall tumor growth as assessed by log-normal mean or tumor sizes up to the 95%
238 percentile tumor (**Supplementary Fig. S10A**). Inactivation of several other genes also had much
239 more significant and dramatic effects on relative tumor burden than on tumor sizes
240 (**Supplementary Fig. S10B and C**). These disproportionate increases in relative tumor burden
241 could be driven by genotype-specific increases in tumor number and/or the sizes of the very
242 largest tumors, neither of which are captured well by log-normal mean or tumor sizes at defined
243 percentile of the tumor size distribution.

244

245 **Many tumor suppressors constrain tumor initiation**

246 Our experimental design, in which we initiated tumors in cohorts of *KT;H11^{LSL-Cas9}* and
247 *KT* mice with the exact same pool of lentiviral vectors, enabled us for the first time to use Tuba-
248 seq to uncover the impact of each putative tumor suppressor gene on tumor initiation and very
249 early oncogenic KRAS-driven epithelial expansion (**Supplementary Fig. S4C and Methods**).
250 The genetic alterations that drive the development of very early epithelial expansions are poorly
251 understood, yet these events influence tumor incidence and set the stage for all subsequent events
252 during cancer evolution. *In vivo* mouse models are particularly well suited to study the effects of
253 genetic alterations on these early events.

254 Fifteen weeks after tumor initiation, inactivation of many genes including *Lkb1*, *Setd2*,
255 and *Stag2*, which had some of the most dramatic effects on tumor growth, did not increase tumor
256 number (defined as the number of clonal expansions with more than 200 cells; **Fig. 5A**;
257 **Supplementary Fig. S4C and Methods**). However, *Pten* inactivation increased tumor number
258 by ~4-fold, suggesting that at least three-quarters of epithelial cells expressing oncogenic
259 KRAS^{G12D} fail to expand beyond a very small size if at all (**Fig. 5A and B**). *Tsc1* inactivation
260 also increases tumor number, albeit to a lesser extent, consistent with TSC1 suppressing mTOR
261 downstream of PI3K (49). Inactivation of *Nfl1*, *Rasa1*, and *p53* also increased tumor number, thus
262 implicating several signaling pathways in the earliest stages of lung tumor development (**Fig.**
263 **5A**). Strikingly, inactivation of four members of the COMPASS complex (*Kdm6a*, *Ncoa6*,
264 *Kmt2c/Mll4* and *Kmt2d/Mll3*) (50,51) all increased tumor number (**Fig. 5A**). The importance of
265 histone H3K4 methylation mediated by this complex is further substantiated by the mutation of
266 at least one member of this complex in 8.9–32.5% of human lung adenocarcinoma (**Fig. 5C and**
267 **D**) (2). Importantly, genes that limit tumor initiation and those that constrain tumor growth are

268 often independent, suggesting that these facets of tumor suppression can represent distinct
269 functions (**Supplementary Fig. S11A**).

270 Analysis of the effect of each genotype on tumor number in mice with tumors initiated
271 with the Lenti-sg85/Cre pool (at both 15 and 26-weeks after tumor initiation) provided us with
272 the opportunity to further validate the effect of tumor suppressor inactivation on tumor initiation
273 and early growth (**Fig. 5E; Supplementary Fig. S11B and C**). The effects of inactivating each
274 tumor suppressor gene on relative tumor numbers were highly correlated across all three datasets
275 (**Fig. 5F; Supplementary Fig. S11D and E**). Several genes including *Cdkn2a*, *Dnmt3a*, *Kdm6a*
276 and *Ncoa6* that initially only increased tumor number also increased overall growth fitness at the
277 later time point. This observation suggests some link between the cellular changes that enable
278 normal epithelial cells to break through the constraints of early hyperplastic growth and the
279 greater fitness in the resulting tumors (**Fig. 4F and 5F; Supplementary Fig. S9B**).

280

281 **Tumor suppressor inactivation allows the emergence of rare but very large tumors**

282 Next, we took advantage of the per-tumor resolution of our Tuba-seq data to quantify the
283 impact of inactivating each gene on the generation of exceptionally large tumors. In addition to
284 the effects of tumor suppressor gene inactivation on overall tumor growth and tumor initiation,
285 the development of exceptionally large tumors is suggestive of genotypes that promote or allow
286 additional alterations to drive aggressive tumor growth. We previously found that one major
287 effect of *p53* deficiency is the generation of such exceptionally large tumors (26,27). Using
288 metrics such as the Hill's estimator (a measure of the heavy-tailedness of a distribution)(52), we
289 quantified the extent to which *p53* inactivation enables the emergence of infrequent but
290 exceptionally large tumors after 15 weeks of tumor growth (**Fig. 6A and B; Supplementary Fig.**

291 **S12A).** The effect of *p53* inactivation is consistent with many previous reports documenting the
292 emergence of large lung tumors in *Kras*^{LSL-G12D/+}; *p53*^{fl/fl} mice (32,53-55). These analyses also
293 showed that inactivation of *Cdkn2a* and the DNA methyltransferase *Dnmt3a*, might allow some
294 tumors to grow to disproportionately large sizes (**Fig. 6A and B; Supplementary Fig. S12A**).

295 To further investigate the effects of tumor suppressor gene inactivation on the emergence
296 of exceptionally large tumors, we determined which genotypes generate heavy-tailed tumor size
297 distribution after 26 weeks of tumor growth. Analysis of the distributions of tumor sizes
298 specifically highlighted the development of exceptionally large *Dnmt3a* and *Cdkn2a*-targeted
299 tumors (**Fig. 6C-E; Supplementary Fig. S12B-D**). Both sgRNAs targeting *Cdkn2a* are
300 anticipated to inactivate both INK4A and ARF, therefore the effect of *Cdkn2a* inactivation could
301 reflect the combined reduction of the Rb and p53-pathways, consistent with our observation that
302 p53 inactivation generates a heavy-tailed distribution (**Fig. 6A and B; Supplementary Fig.**
303 **S12A**)(26,27). The emergence of very large *Cdkn2a*- and *Dnmt3a*-deficient tumors is consistent
304 with the increased lung tumor burden in oncogenic *Kras*^{LSL-G12D}-driven tumors with Cre/lox
305 mediated inactivation of these genes (56,57). However, the per-tumor resolution of our data
306 suggests that the inactivation of INK4A/ARF or the DNA-methyltransferase DNMT3A enables
307 the emergence of rare but exceptionally large tumors, while having only a modest impact on the
308 growth of the vast majority of tumors (**Fig. 6E; Supplementary Fig. S12C**). Therefore, the role
309 of tumor suppressors in preventing the development of exceptionally large tumors can be
310 independent of their roles in regulating tumor initiation and overall growth during cancer
311 evolution.

312

313 **Limited effects of overall tumor burden and sex on tumor suppressor function**

314 Our high-resolution data across multiple facets of tumor suppression in principle allow
315 for quantification of the effects of other variables on tumor suppressor effects. Given that overall
316 tumor burden varies across mice and that we initiated tumors in mice of both sexes, we assessed
317 how these variables influence tumor suppressor effects. To uncover whether overall tumor
318 burden influences genotype-specific effects, we divided our *KT;H11^{LSL-Cas9}* mice with Lenti-
319 sg*TS102*/Cre-initiated tumors into three groups with low, medium, and high tumor burden and
320 reassessed multiple metrics of tumor initiation and growth (**Supplementary Fig. S13A**). Very
321 few genotype-specific tumor-suppressive effects were influenced by overall tumor burden,
322 suggesting that our results are largely unaffected by potential differences in paracrine or physical
323 interactions that change with tumor density (**Supplementary Fig. S13B-E**).

324 There is a growing interest in understanding sex-specific effects on all aspects of
325 carcinogenesis. Our data derived from both male and female mice allowed us to investigate sex-
326 specific differences in tumor suppression. Inactivation of most genes, including those on the X
327 chromosome, had similar effects on tumor growth and tumor number in male and female mice
328 (**Supplementary Fig. S14A-D**). Thus, tumor suppressor effects in lung cancer are not
329 dramatically impacted by differences in the host environment driven by sex. This was
330 particularly illuminating for *Kdm6a*, which is an X-linked gene that has both H3K27me3
331 demethylase and non-enzymatic functions (58). Its non-enzymatic function can be compensated
332 for by its paralog UTY on the Y chromosome, and thus different effects in male and female mice
333 have been used to provide insight into the molecular function of KDM6A (58). *Kdm6a*
334 inactivation increased tumor number similarly in male and female mice. The effects were
335 consistent in our data at 15 and 26 weeks after tumor initiation, suggesting that the impact of

336 KDM6A inactivation is most likely driven by loss of its enzymatic function (**Supplementary**
337 **Fig. S14E-H**).

338

339 **Evaluation of sensitivity and specificity**

340 To better estimate the impact of false negatives and false positives on our data, we used
341 all of our datasets to estimate the true positive rate (**Methods**). Within all of our datasets, the
342 effects of sgRNAs targeting the same gene were concordant across multiple metrics, consistent
343 with on-target effects (**Fig. 2 and 4; Supplementary Fig. S15A-F**). For instance, in our
344 experiment using Lenti-sg*TS102*/Cre pool, when one sgRNA showed a significant tumor
345 suppressive effect (nominal $P < 0.05$), the probability to re-detect the significant effect using the
346 other guide was above 89% for all metrics assessed (**Supplementary Table S3**). Thus, the
347 probability that both sgRNAs fail to uncover a functional tumor suppressor that has a similar
348 effect to the tumor suppressors identified in our analysis is below 5% (**Supplementary Table**
349 **S3**). Note that for the eight major tumor suppressor genes that were excluded from the Lenti-
350 sg*TS85*/Cre Pool, significant effects for both sgRNAs were uncovered in every case. Given these
351 results and the targeting of each putative tumor suppressor gene with two sgRNAs, it is unlikely
352 that functional tumor suppressors were missed for technical reasons. Furthermore, analysis of
353 sgRNA cutting in cells in culture showed comparable efficiency of sgRNAs targeting genes that
354 emerged as tumor suppressors and those that did not (**Supplementary Fig. S15G-I**). Finally,
355 power calculations using our data suggest that an even larger number of genes could be assessed
356 using reasonable numbers of mice using these methods (**Supplementary Fig. S16A-C**).

357

358 **Human mutational data, cell line studies, and *in vivo* functional studies are complementary**
359 **in defining a catalog of tumor suppression**

360 The candidate tumor suppressor genes that we assessed were chosen based on existing
361 human mutational data; however, each gene has different levels of correlative data supporting its
362 function as a tumor suppressor (**Supplementary Table S1**). We explored whether effects on
363 tumorigenesis within the autochthonous environment could be predicted by either human
364 mutation data or through the analysis of human cell lines. Several strong functional tumor
365 suppressors did not stand out based on the human mutational frequency data, and genes such as
366 *STAG2*, *CMTR2*, and *CDKN2C* were not often predicted to be tumor suppressor genes based on
367 human mutational data (**Fig. 2A; Supplementary Fig. S17A-G**). Thus, computational
368 predictions of tumor suppressor function from mutational data alone (including statistical
369 methods that already integrate background mutation rate corrections as well as function- and
370 structure-based impact predictions) nominate some but not all functional tumor suppressors.

371 Analysis of data from the Dependency Map (59), in which genome-scale knockout
372 screens were performed across diverse cancer cell lines, was also revealing. Inactivation of
373 several top functional tumor suppressors, including *PTEN*, *CDKN2C*, *RBL*, and *RNF43* increased
374 lung adenocarcinoma cell line growth as expected (**Supplementary Fig. S17H**). However,
375 inactivation of several other major functional tumor suppressors, including *LKB1*, *SETD2*, and
376 *STAG2* paradoxically decreased cancer cell growth in culture (**Supplementary Fig. S17H**). The
377 effects of inactivating several modest tumor suppressors were concordant between the human
378 cell lines and *in vivo* mouse model data, although inactivation of some genes, including *CMTR2*,
379 *RBM10*, and *KEAP1*, had variable or growth-suppressive effects on cancer cells in culture (**Fig.**

380 **4B; Supplementary Fig. S17H).** Collectively, these results underscore the differences in the
381 fitness landscape in cell lines and indicate that *in vivo* studies can complement these analyses.

382

383 **DISCUSSION**

384 The enormous genomic diversity in cancer, even within tumors of the same subtype,
385 creates a challenge for identifying driver genes and deciphering their roles in tumor
386 development. Given the sample sizes of cancer genome sequencing studies, variation in genomic
387 features such as gene length and mutation rate will continue to make computational predictions
388 of tumor suppressor function from mutation data difficult, except for a subset of genes (9,60,61).

389 Moreover, mutation frequencies alone cannot easily define the importance of each tumor
390 suppressor gene and even less so be used to glean their mode of action. Indeed, even rarely
391 mutated tumor suppressor genes can have large consequences when inactivated, with the rarity of
392 mutation being driven by mutational cold spots, epistatic interactions and biological context
393 (9,62) rather than by the magnitude of their inhibitory function (**Supplementary Fig. S17A**).

394 Thus, while experiments using model organisms could be impacted by species-specific effects, *in*
395 *vivo* functional studies that include autochthonous tumor initiation, growth and progression are
396 an important complement to the computational investigation of tumor suppressor inactivation in
397 human tumors (13,20,21).

398 Carcinogenesis is broadly impacted by different aspects of the *in vivo* environment. By
399 enhancing the throughput, sensitivity, and precision of Tuba-seq (26,27), we quantify the effects
400 of inactivating a diverse panel of putative tumor suppressor genes in an autochthonous mouse
401 model of oncogenic KRAS-driven lung cancer. The parallel analysis of ~50 different genotypes
402 not only uncovered previously uncharacterized functional tumor suppressor genes but also

403 provided new insights into the landscape of tumor suppression and multiple modes of action of
404 tumor suppressor genes (**Fig. 7A and B**). We show that tumor suppression is unexpectedly
405 complex and multi-faceted, with some genes suppressing tumor initiation, some constraining
406 overall tumor growth, and others limiting the emergence of a small proportion of unusually fast-
407 growing tumors (**Fig. 7A and B**). Furthermore, while some genes affect only a single feature of
408 carcinogenesis, others affect multiple facets of tumor evolution to varying extents (**Fig. 7C**). The
409 relative importance of these genes can also change during the course of carcinogenesis (**Fig. 7B**
410 and **C**). Understanding the impact of tumor suppressors that primarily regulate certain aspects of
411 carcinogenesis may have a unique value for cancer prevention, early detection, and therapeutic
412 targeting. The discovery of such functional complexity points to shifting challenges during
413 different stages of carcinogenesis. Thus, tumor suppressors are not simply “brakes” on
414 proliferation but rather contextually and temporally dependent genetic modifiers of different
415 phases of carcinogenesis.

416 Our results are largely consistent with previous studies that assessed some of these genes
417 individually using similar *in vivo* mouse models of lung cancer (22,26,31-34,51,63,64).
418 However, single-gene approaches and quantification of overall tumor burden alone are limited in
419 their ability to uncover the modes of tumor suppression and do not enable direct comparison
420 across many genotypes. For example, while *Lkb1*, *Pten*, *Kdm6a*, *Dnmt3a* and *p53* inactivation
421 each increase overall tumor burden, our quantitative, multiplexed design and computational
422 platform uniquely enabled the deconvolution of different aspects of tumor suppression (**Fig. 7A**).

423 We show that the inactivation of many understudied genes has major effects on tumor
424 growth (**Fig. 7C; Supplementary Fig. S3**). Identifying additional genes that are fundamentally
425 important in suppressing carcinogenesis, including those that are less frequently mutated in

426 human lung adenocarcinoma, can highlight key molecular and cellular processes that are critical
427 in cancer. Furthermore, alterations in cis-regulatory elements, epigenetic silencing and mutations
428 in other members of the same complexes or pathways likely dysregulate these processes in a
429 much higher percentage of tumors. Thus, these types of *in vivo* findings suggest not only the
430 importance of certain genes but also more broadly uncover under-appreciated cellular processes
431 that limit cancer development. Our findings nominate several novel genes and key pathways that
432 should be investigated in further mechanistic detail. In particular, the mechanisms by which
433 STAG2 inactivation drives lung cancer growth remain to be elucidated.

434 One key approach used to implicate the context-dependency of tumor suppressor function
435 is the analysis of mutual exclusivity in human data (65). Interestingly, our data demonstrate that
436 genes that trend toward mutual exclusivity with oncogenic *KRAS* mutations, such as *NF1* and
437 *PTEN* are still important suppressors of oncogenic KRAS-driven lung cancer (**Supplementary**
438 **Fig. S17B**). Such statistical trends toward mutual exclusivity should not be misinterpreted as the
439 lack of tumor-suppressive effect of these genes in oncogenic KRAS-driven lung cancer, and
440 more generally, these types of patterns in mutation data should be interpreted with caution (66).
441 Instead, these patterns likely reflect complex epistatic interactions in which context-dependence
442 drives frequencies and mutation spectra (9,62).

443 Our data, coupled with human lung adenocarcinoma sequencing studies, provide the most
444 comprehensive map of *in vivo* tumor suppressor gene function for cancer (**Fig. 7C**). Given the
445 quantitative and cost-effective nature of Tuba-seq, even broader studies of many other genes and
446 combinations of genomic alterations may be warranted. Moreover, studies across different
447 genetic and environmental contexts may further elucidate and refine the modality and context-
448 dependence of tumor suppressor gene effects (27,67,68). This should lead to a more thorough

449 understanding of the interactions between cell-intrinsic and extrinsic processes that contribute to
450 the etiology and evolution of lung cancer.

451

452 **ACKNOWLEDGEMENTS**

453 We thank the Stanford Shared FACS Facility for flow cytometry and cell sorting
454 services, the Stanford Veterinary Animal Care Staff for expert animal care, Human
455 Pathology/Histology Service Center, Stanford Protein and Nucleic Acid Facility, the Francis
456 Crick Genomics Equipment Park, Advanced Sequencing Facility, Bioinformatics & Biostatistics
457 and Y. Zhao, D. Maghini, and R. Ma for experimental support; A. Orantes for administrative
458 support; R. Levine's laboratory for making the *Stag2*^{fl/fl} allele available prior to publication; D.
459 Feldser, J. Sage, and members of the Winslow, Petrov, and Swanton laboratories for helpful
460 comments. H.C. was supported by a Tobacco-Related Disease Research Program (TRDRP)
461 Postdoctoral Fellowship (28FT-0019). S.K.C. was supported by the European Research Council
462 (ERC) under the European Union's Seventh Framework Programme (FP7/2007-2013)
463 Consolidator Grant (THESEUS). C.L. is the Connie and Bob Lurie Fellow of the Damon
464 Runyon Cancer Research Foundation (DRG-2331). C.W.M. was supported by the NSF Graduate
465 Research Fellowship Program and an Anne T. and Robert M. Bass Stanford Graduate
466 Fellowship. N.W.H. was supported by the NSF Graduate Research Fellowship Program. R.T.
467 was supported by a Stanford University School of Medicine Dean's Postdoctoral Fellowship and
468 a TRDRP Postdoctoral fellowship (27FT-0044). M.Y. was supported by a Stanford University
469 School of Medicine Dean's fellowship, an American Lung Association senior research training
470 grant, and NIH Ruth L. Kirschstein National Research Service Award (F32-CA236311). C.D.M.
471 was supported by NIH K99-CA226506. W-Y.L. was supported by an American Association of

472 Cancer Research Postdoctoral fellowship (17-40-18-LIN). C.S. is Royal Society Napier Research
473 Professor (RP150154). This work was supported by the Francis Crick Institute that receives its
474 core funding from Cancer Research UK (FC001169), the UK Medical Research Council
475 (FC001169), and the Wellcome Trust (FC001169). This research was funded in part by the
476 Wellcome Trust (FC001169 to C.S.), and by a Stand Up To Cancer-LUNGevity-American Lung
477 Association Lung Cancer Interception Dream Team Translational Cancer Research Grant (Grant
478 Number: SU2C-AACR-DT23-17). Stand Up To Cancer is a division of the Entertainment
479 Industry Foundation. The indicated SU2C research grant is administered by the American
480 Association for Cancer Research, the scientific partner of SU2C. C.S. is funded by Cancer
481 Research UK (TRACERx, PEACE and CRUK Cancer Immunotherapy Catalyst Network),
482 Cancer Research UK Lung Cancer Centre of Excellence, the Rosetrees Trust, Butterfield and
483 Stoneygate Trusts, NovoNordisk Foundation (ID16584), Royal Society Professorship
484 Enhancement Award (RP/EA/180007), the National Institute for Health Research (NIHR)
485 Biomedical Research Centre at University College London Hospitals, the CRUK-UCL Centre,
486 Experimental Cancer Medicine Centre, and the Breast Cancer Research Foundation (BCRF,
487 USA). C.S. receives funding from the European Research Council (ERC) under the European
488 Union's Seventh Framework Programme (FP7/2007-2013) Consolidator Grant (FP7-THESEUS-
489 617844), European Commission ITN (FP7-PloidyNet 607722), an ERC Advanced Grant
490 (PROTEUS) from the European Research Council under the European Union's Horizon 2020
491 research and innovation programme (Grant 835297), and Chromavision from the European
492 Union's Horizon 2020 research and innovation programme (Grant 665233). This work was
493 supported by NIH R01-CA207133 (to M.M.W and D.A.P.), NIH R01-CA231253 (to M.M.W

494 and D.A.P), NIH R01-CA234349 (to M.M.W and D.A.P.), and in part by the Stanford Cancer
495 Institute support grant (NIH P30-CA124435).

496

497 **CONTRIBUTIONS**

498 H.C., S.K.C., C.L., M.M.W., C.S., and D.A.P. designed the project. H.C. and S.K.C.
499 generated the lentiviral vector pool and initiated lung tumors in mice. H.C, M.K.T. and R.T. bred
500 the mice. H.C., S.K.C., C.L., M.K.T., L.A., C.W.M., R.T., K.L.H., L.C.C. and M.Y. collected lung
501 samples. L.A., E.L.A. and K.L.H. performed immunohistochemical staining. H.C., S.K.C., L.A.,
502 C.W.M. and W.Y.L. generated the barcode sequencing library. C.L. and E.G.S. analyzed the Tuba-
503 seq data. N.W.H. and L.C. analyzed DepMap and indel data. S.K.C., L.C.C., S.Y.C.L. and C.D.M.
504 analyzed the human datasets. C.A.K. analyzed the tumor histology. H.C., S.K.C., C.L., D.A.P. and
505 M.M.W. wrote the manuscript with comments from all authors.

506

507 **METHODS**

508 **Selection of candidate tumor suppressor genes for this study**

509 To select candidate genes to assess *in vivo* using Tuba-seq (and to complement genomics
510 and cell biology approaches), we generated a highly human-curated panel that integrating many
511 different considerations.

512 Known lung adenocarcinoma driver tumor suppressors genes at >5% mutational
513 frequency (such as *P53*, *LKB1*, *CDKN2A*, *KEAP1*) from The Cancer Genome Atlas (TCGA),
514 AACR Project Genomics, Evidence, Neoplasia, Information, Exchange (GENIE), and TRAcking
515 Cancer Evolution through therapy (Rx) (TRACERx) datasets which were previously assessed by

516 Tuba-seq were included as positive controls. We included genes that tend to co-occur with
517 oncogenic *KRAS* mutations and those that do not. We also included genes that have been
518 categorized as tumor suppressor genes in other cancer types with >5% mutational frequency in
519 lung (such as *KDM6A* and *FAT1*), even if they are not predicted to be involved in lung
520 adenocarcinoma (**Fig. 1A**; **Supplementary Fig. S1** and **Table S1**).

521 We also considered the distribution of mutations within genes (**Fig. 1B**), including low
522 mutation frequency genes (<5%) that show potential clonal or subclonal bias from the
523 TRACERx dataset (**Supplementary Table S1**), genes with discrepancies in scoring of potential
524 driver activity (**Supplementary Fig. S2**), as well as genes that represent biological processes or
525 functions commonly associated with carcinogenesis (**Supplementary Fig. S3**). From a curated
526 survey of literature, candidate genes that have been discussed as cancer driver genes without
527 much or any functional data were also included (**Supplementary Fig. S4**).

528

529 **Analysis of human lung adenocarcinoma cancer genome sequencing data**

530 Mutation frequencies and other information for the 48-gene panel of putative candidate
531 tumor suppressor genes are available from multiple cancer datasets and their analyses in
532 TRACERx (6), GENIE (2) and TCGA (7,69,70). Oncogenes are characterized by missense point
533 mutations arising in mutational hotspots. In contrast, TSGs are characterized by protein
534 truncating mutations (nonsense and frameshifts) that are more dispersed across the transcript.
535 Moreover, when nonsense and frameshift mutations arise in oncogenes, they tend to truncate C-
536 terminal domains and occur towards the end of the transcript. To identify putative TSGs, we
537 characterized all genes in this survey by these two genetic features: mutational hotspots and the
538 fraction of protein truncated per mutation. We used all point mutations and short insertion and

539 deletions found within the TCGA lung adenocarcinoma (7) and Catalogue Of Somatic Mutations
540 In Cancer (COSMIC)(71) databases. The extent of mutational hotspots within a gene was
541 determined using a normalized measure of dispersion (Green's Contagion) of the number of
542 missense mutations observed within all five residue rolling windows in each gene:
543 $(\sigma^2/\mu - 1)/(\mu N - 1)$, where μ is the mean number of missense mutations observed within each
544 window, σ^2 is the unbiased estimator of the variance, and N is the number of missense mutations.
545 Green's Contagion and the five-residue window size and were chosen because they maximized
546 the accuracy of classification of known oncogenes and tumor suppressors. Larger values of
547 Green's Contagion suggest that mutations are clumping at a few residues within the protein and
548 that the mutant gene is likely oncogenic. This measure has a value of zero when mutations are
549 randomly dispersed throughout the gene and can be negative when mutations are under-
550 dispersed. The fraction of protein truncated per mutation is the mean number of amino acids lost
551 per nonsynonymous mutation. It is calculated by simply averaging the fraction of a transcript lost
552 due to each frameshift and nonsense mutation, while assigning a value of zero to all missense
553 mutations in this collective average.

554 To summarize what has previously been described about the biological functions of the
555 candidate genes, we used driver gene scores from attempts to discover cancer driver genes using
556 multiple approaches, such as weighted consensus across multiple tools (8) and prediction by
557 machine learning (29). We also collated the known biological processes and subcellular
558 localization of the 48 genes from the Gene Ontology database (release date 2019-07-01)(30).

559 For co-occurrence of mutations in *KRAS* and each selected gene, the odds ratio (equals
560 $(N_{\text{neither were mutated}} * N_{\text{Both were mutated}}) / (N_{\text{only KRAS is mutated}} * N_{\text{only selected gene is mutated}})$) and *P*-value
561 (one-sided Fisher's Exact Test) were available on cBioPortal.org. 566 lung adenocarcinoma

562 cases from TCGA Pan-cancer Atlas and 8522 lung adenocarcinoma samples from GENIE were
563 analyzed. Note that *NCOA6*, *ATF7IP*, *CMTR2* and *UBR5* are not profiled in any GENIE lung
564 adenocarcinoma cases and hence were excluded from the analysis. For the fitting of a simple
565 linear regression between measured phenotypes and observed clinical parameters, we used data
566 from mutation timing and clonality in lung adenocarcinomas that have been previously described
567 (6,70).

568

569 **Analysis of publications suggesting tumor suppressive function of each putative tumor
570 suppressor gene in lung cancer**

571 List of articles related to the gene was accessed through the “Bibliography” section of
572 NCBI Gene (<https://www.ncbi.nlm.nih.gov/gene/>). Subsequently, “lung cancer” and/or “tumor
573 suppressor” were used as the keywords to refine the search.

574

575 **Calculation of gene inclusion in gene sequencing panels**

576 GENIE panel sequencing information was compiled through the GENIE 6.1 Public
577 Release. We first generated a list of panels that provided data from patients with “Cancer Type
578 Detailed” listed as “Lung Adenocarcinoma”, “Lung Adenocarcinoma In Situ”, or “Lung
579 Adenosquamous Carcinoma” by filtering the data_clinical_sample.txt file. Then, by parsing the
580 genie_combined.bed file, we generated a list of “screened” genes for each panel, which refers to
581 genes that have “Feature_Type” listed as “exon” and “includeInPanel” listed as “True”. This list
582 was then utilized to categorize our pool of tumor suppressors as either “screened” or
583 “unscreened” by these sequencing panels. Stanford Solid Tumor Actionable Mutation Panel
584 (STAMP) and FoundationOne CDx sequencing panels were obtained from the official websites.

585

586 **Design, generation, barcoding, and production of lentiviral vectors**

587 The sgRNA sequences targeting the putative tumor suppressor genes were designed using
588 Desktop Genetic's Guide Picker (72) (<https://www.deskgen.com/guide-picker>) to prioritize on-
589 target activity (score of >0.6)(73), specificity (score of >0.6)(74), likelihood of generating
590 frameshift indels (score of >0.6)(75), targeting of maximal number of transcript isoforms, no
591 homopolymer runs in the sgRNA, and no extremes in GC-content of sgRNA (0.4-0.75), as
592 detailed in **Supplementary Table S2**.

593 The Lenti-U6-sgRNA-sgID-barcode-Pgk-Cre vector was modified from our previous
594 work (26) as follows. The sgRNA sequence of the previously described pLenti-sgNT1/Cre
595 (Addgene #66895) vector was replaced with GCGAGGTATTACCGGCGTATCATCCGCG by
596 site-directed mutagenesis to generate pLenti-BaeI-Pgk-Cre. The replacement sequence contains a
597 recognition site for the Type IIS restriction endonuclease BaeI, allowing for quick replacement
598 of the sgRNA sequence. To generate each desired vector, forward and reverse single-stranded
599 oligonucleotides containing the sgRNA sequence and complementary overhangs is annealed and
600 ligated into the BaeI-linearised pLenti-BaeI-Pgk-Cre vector using T4 DNA ligase. The barcode
601 oligo primer contains the 8-nucleotide sgID sequence and 20-nucleotide degenerate barcode
602 (**Supplementary Table S2**). The generation of the barcode fragment and subsequent ligation
603 into the vectors were performed as previously described (26).

604 Lenti-sgRNA/Cre vectors were individually co-transfected into 293T cells with pCMV-
605 VSV-G (Addgene #8454) envelope plasmid and pCMV-dR8.2 dvpr (Addgene #8455) packaging
606 plasmid using polyethylenimine. Supernatants were collected at 48 and 72 hours after
607 transfection, filtered through a 0.45 µm syringe filter unit (Millipore SLHP033RB) to remove

608 cells and debris, concentrated by ultracentrifugation (25,000 g for 1.5 hours at 4°C), and
609 resuspended in PBS. Each virus was titered against a standard of known titer using LSL-YFP
610 Mouse Embryonic Fibroblasts (MEFs) (a gift from Dr. Alejandro Sweet-Cordero/UCSF). These
611 MEFs and 293T cells were regularly tested with MycoAlert mycoplasma detection kit (Lonza,
612 cat# LT07-418) to make sure that they are free of mycoplasma. All lentiviral vector aliquots
613 were stored at -80°C and were thawed and pooled at equal ratios immediately prior to delivery to
614 mice.

615

616 **Mice and tumor initiation**

617 The use of mice for the current study has been approved by Institutional Animal Care and
618 Use Committee at Stanford University, protocol number 26696.

619 *Kras*^{LSL-G12D/+} (RRID:IMSR_JAX:008179), *R26*^{LSL-*tdTomato*} (RRID:IMSR_JAX:007909),
620 and *H11*^{LSL-Cas9} (RRID:IMSR_JAX:027632) mice have been previously described (24,76,77).
621 They were on a C57BL/6:129 mixed background. The *Stag2*^{tm1c(EUCOMM)Wtsi/J} (*Stag2*^{flox}) mice
622 were initially generated by Viny *et al.*(42) and obtained from the Jackson Laboratory
623 (RRID:IMSR_JAX:030902). Tumors were initiated by intratracheal delivery of 60 µl of
624 lentiviral vectors dissolved in PBS.

625 For the initial experiments, tumors were allowed to develop for 15 weeks after viral
626 delivery of a lentiviral pool that contained 102 barcoded Lenti-sgRNA/Cre vectors (Lenti-
627 sgTS102/Cre). Tumors were initiated in *Kras*^{LSL-G12D}; *R26*^{LSL-Tom/LSL-Tom} (*KT*) mice with 9x10⁴
628 infectious units (ifu)/mouse of the Lenti-sgTS102/Cre pool (12 mice analyzed at 15 weeks after
629 tumor initiation), and in *KT;H11*^{LSL-Cas9/LSL-Cas9} mice with 3x10⁴ ifu/mouse of the Lenti-
630 sgTS102/Cre pool (47 mice analyzed at 15 weeks after tumor initiation).

631 After the detection of the top functional tumor suppressors after 15 weeks of tumor
632 development, tumors were initiated in additional mice using a sub-pool of 85 Lenti-sgRNA/Cre
633 vectors (Lenti-sg*TS85*/Cre), which excluded the vectors targeting *Cdkn2c*, *Lkb1*, *Nfl*, *p53*, *Pten*,
634 *Rb1*, *Setd2*, and *Stag2*. Tumors were initiated in *KT* mice with 2.5×10^5 ifu/mouse (6 mice
635 analyzed at 15 weeks after tumor initiation), *KT;H11^{LSL-Cas9}* mice with 6×10^4 ifu/mouse (10 mice
636 analyzed at 15 weeks after tumor initiation), and *KT;H11^{LSL-Cas9}* mice with 1.5×10^4 ifu/mouse
637 (40 mice analyzed at 26 weeks after tumor initiation).

638 For the validation experiments using Lenti-sgRNA/Cre-mediated gene inactivation,
639 tumors were allowed to develop for 15 weeks after viral delivery. Tumors were initiated with
640 individual barcoded Lenti-sgRNA/Cre vectors in *KT* mice with 1×10^5 ifu/mouse (3 mice per
641 vector analyzed at 15 weeks after tumor initiation), and *KT;H11^{LSL-Cas9}* mice with 1×10^5
642 ifu/mouse (5-6 mice per vector analyzed at 15 weeks after tumor initiation).

643 For the survival experiments using Lenti-sgRNA/Cre-mediated gene inactivation, tumors
644 were allowed to develop until humane endpoints. Tumors were initiated in *KT;H11^{LSL-Cas9}* mice
645 with individual barcoded Lenti-sg*Inert*/Cre vectors at 2×10^4 ifu/mouse and with individual
646 barcoded Lenti-sg*Stag2*/Cre vectors at 1×10^4 ifu/mouse (7 mice per vector analyzed).

647 For *Stag2* validation experiments using the *Stag2^{floxed}* allele, tumors were initiated with
648 Lenti-sg*Inert*/Cre in *KT*, *KT;Stag2^{flox/+}*, *KT;Stag2^{flox/flox}* and *KT;Stag2^{flox/y}* mice with 1×10^5
649 ifu/mouse (4-5 mice per group analyzed) and allowed to develop for 15 weeks, and *KT*,
650 *KT;Stag2^{flox/+}*, *KT;Stag2^{flox/flox}* and *KT;Stag2^{flox/y}* mice with 1×10^5 ifu/mouse (6-7 mice per
651 genotype analyzed) and allowed to develop until humane endpoints.

652

653 **Tuba-seq library generation**

654 Genomic DNA was isolated from bulk tumor-bearing lung tissue from each mouse as
655 previously described (26). Briefly, benchmark control cell lines were generated from LSL-YFP
656 MEFs transduced by a barcoded Lenti-sgNT3/Cre vector (NT3: an inert sgRNA with a distinct
657 sgID) and purified by sorting YFP⁺ cells. For mice initiated with Lenti-sgTS102/Cre pool, twelve
658 benchmark control cell lines (3 cell lines of 500,000 cells each, 3 cell lines of 50,000 cells, 3 cell
659 lines of 5,000 cells, and 3 cell lines of 500 cells) were added to each mouse lung sample prior to
660 lysis to enable the calculation of the absolute number of neoplastic cells in each tumor from the
661 number of sgID-BC reads. Because the standard curve was highly linear, we reduced the
662 benchmark controls to three cell lines with 500,000 cells each for the Lenti-sgTS85/Cre pool.
663 Following homogenization and overnight protease K digestion, genomic DNA was extracted
664 from the lung lysates using standard phenol-chloroform and ethanol precipitation methods.

665 Subsequently, Q5 High-Fidelity 2x Master Mix (New England Biolabs, M0494X) was
666 used to amplify the sgID-BC region from 32 µg of genomic DNA. The unique dual-indexed
667 primers used were *Forward*: AATGATA CGGC GACC ACCGAG ATCTACAC-8 nucleotides for
668 i5 index-ACACTTTCCCTACACGACGCTCTTCCGATCT-6 to 9 random nucleotides for
669 increased diversity-GCGCACGTCTGCCGCGCTG and *Reverse*:
670 CAAGCAGAAGACGGCATACGAGAT-6 nucleotides for i7 index-
671 GTGACTGGAGTTCA GACGTGTGCTCTTCCGATCT-9 to 6 random nucleotides for
672 increased diversity-CAGGTTCTTGC GAA CCTCAT. The PCR products were purified with
673 Agencourt AMPure XP beads (Beckman Coulter, A63881) using a double size selection
674 protocol. The concentration and quality of the purified libraries were determined using Agilent
675 High Sensitivity DNA kit (Agilent Technologies, 5067-4626) on the Agilent 2100 Bioanalyzer
676 (Agilent Technologies, G2939BA). The libraries were pooled based on lung weight to ensure

677 even reading depth, cleaned up again using AMPure XP beads, and sequenced (read length
678 2x150bp) on the Illumina HiSeq 2500 or NextSeq 550 platform (Admera Health Biopharma
679 Services).

680

681 **Code and data availability**

682 Python 3.6 and R 3.6 were used for analyzing the data. The codes are available on
683 GitHub, link: <https://github.com/lichuan199010/functional-taxonomy-of-tumor-suppressors>

684 The data sets generated and analyzed in the current study are available in the NCBI Gene
685 Expression Omnibus database, token: ezsjeksixhkvbqh, link:
686 <https://www.ncbi.nlm.nih.gov/geo/query/acc.cgi?acc=GSE146302>

687

688 **Process paired-end reads to identify the sgID and barcode**

689 The FASTQ files were parsed to identify the sgID and barcode for each read. Each read
690 is expected to contain an 8-nucleotide sgID region followed by a random nucleotide barcode
691 region (**GCNNNNNTANNNNNGCNNNNNTANNNNNGC**), and each of the 20 Ns represents
692 random nucleotides. The sgID region identifies the putative tumor suppressor gene being
693 targeted, for which we require a perfect match between the sequence in the forward read and one
694 of the 102 sgIDs with known sequences. Note that all sgID sequences differ from each other by
695 at least three nucleotides. Therefore, the incorrect assignment of sgID due to PCR or sequencing
696 error is extremely unlikely. All cells in a clonal expansion from a cell transduced by a lentiviral
697 vector carry the same BC sequence. To minimize the effects of sequencing errors on calling the
698 BC, we require the forward and reverse reads to agree completely within the random nucleotide
699 sequence to be further processed. In our pipeline, any “tumor” within a Hamming distance of

700 two from a larger tumor is assigned as “spurious tumors”, which is likely to be resulting from
701 sequencing or PCR errors and is removed from subsequent analysis. Reads with the same sgID
702 and barcode are assigned to be the same tumor. The tumor size (number of neoplastic cells) is
703 calculated by normalizing the number of reads from an individual tumor to the number of reads
704 from the benchmark control cell lines added to each sample prior to lung lysis and DNA
705 extraction. The minimum sequencing depth was ~1 read per 43 cells. We have high statistical
706 power in identifying tumors with over 200 cells, which was used as the minimum cell number
707 cutoff for calling tumors.

708

709 **Summary statistics for overall growth rate**

710 Three summary statistics, relative sizes at defined percentiles, relative log-normal mean
711 and relative tumor burden (will be introduced in a later section), were used to describe the
712 overall tumor growth as previously described. Relative sizes at defined percentiles are
713 nonparametric summary statistics for the tumor size distribution. Specifically, the relative sizes
714 at Xth percentiles are calculated as the Xth percentile (X represents 50% (median), 60%, 70%,
715 80%, 90% and 95%) of the tumor size distribution of sgTS tumors divided by the corresponding
716 percentile of the tumor size distribution of all sgInert tumors. This ratio represents the growth
717 advantage at various percentiles conferred by the inactivation of the tumor suppressor gene.

718 Relative size of tumors at Xth percentile =

$$719 \frac{\text{Neoplastic cell number at the } X^{\text{th}} \text{ percentile for sgTS tumors}}{\text{Neoplastic cell number at the } X^{\text{th}} \text{ percentile for sgInert tumors}}$$

720 Log-normal mean is the maximum likelihood estimator for the mean number of
721 neoplastic cells for sgTS tumors assuming a log-normal distribution of tumor sizes. Similarly, we

722 calculate the relative log-normal mean by dividing the log-normal mean of sgTS tumors by the
723 log-normal mean of the sgInert tumors (**Supplementary Fig. S4**).

724
$$\text{Relative log - normal mean} = \frac{\text{log normal mean for sgTS tumors}}{\text{log normal mean for sgInert tumors}}$$

725

726 **Summary statistics for heavy-tailedness of the tumor size distribution**

727 Some tumor suppressor genes may lead to rare cases of exceptionally large tumors, which
728 results in a tumor size distribution with a heavy tail. We used two summary statistics, relative
729 Hill's estimator and relative steepness to characterize the heavy-tailedness of the tumor size
730 distribution.

731 Hill's estimator is a commonly used tail index to characterizes the tail shape of heavy-
732 tailed distributions (52). Suppose X_1, X_2, \dots, X_n are sgTS tumor sizes, and we order them by size
733 such that $X_1 \geq X_2 \geq \dots \geq X_n$. Let X_k be the tumor size at the 95th %ile, and the Hill's estimator is
734 calculated as,

735
$$H = \frac{1}{k} \sum_{i=0}^k \ln \left(\frac{X_i}{X_k} \right)$$

736 The relative Hill's estimator is calculated by dividing the Hill's estimator for tumors with
737 sgTS by that of tumors with sgInert.

738
$$\text{Relative Hill's estimator} = \frac{H \text{ for sgTS tumors}}{H \text{ for sgInert tumors}}$$

739 The steepness (99th percentile / 95th percentile) is calculated as the ratio of the 99th
740 percentile over the 95th percentile for the tumor size distribution for each sgID. Large values of
741 these estimators indicate that the tumor size distributions are heavy-tailed. We calculate the
742 relative steepness by dividing the steepness of tumors with sgTS by that of tumors with sgInert.

743 Steepness =
$$\frac{\text{Number of neoplastic cells at the 99}^{\text{th}} \text{ percentile for } sgTS \text{ tumors}}{\text{Number of neoplastic cells at the 95}^{\text{th}} \text{ percentile for } sgInert \text{ tumors}}$$

744 Relative steepness =
$$\frac{\text{Steepness for } sgTS \text{ tumors}}{\text{Steepness for } sgInert \text{ tumors}}$$

745 For both relative Hill's estimator and relative steepness, values higher than one indicate
746 that the gene inactivation leads to heavier tail and value smaller than one indicate gene
747 inactivation leads to lighter tail than expected (**Supplementary Fig. S4**).

748

749 **Summary statistics for relative tumor number and relative tumor burden**

750 The four metrics above compare the tumor size distribution of *sgTS* tumors relative to
751 *sgInert* tumors and can be calculated for both *KT;H11^{LSL-Cas9}* mice and *KT* mice, separately.
752 Unlike these size metrics, relative tumor number and relative tumor burden are affected linearly
753 by lentiviral titer. Therefore, when calculating these two metrics, we normalized it to that in
754 *KT* mice to account for the viral titer differences among different Lenti-sgRNA/Cre vectors.

755 We normalized the observed tumor number for *sgTS* tumors in *KT;H11^{LSL-Cas9}* mice by
756 dividing it by that of *sgTS* tumors in *KT* mice to account for the titer differences for each *sgTS*.

757 Tumor number =
$$\frac{\sum \text{tumor number in } KT; H11^{LSL-Cas9} \text{ mice}}{\sum \text{tumor number in } KT \text{ mice}} \text{ for each } sgTS$$

758 The relative tumor number is calculated as the ratio of tumor number for each *sgTS*
759 relative to *sgInert*:

760 Relative tumor number =
$$\frac{\text{Tumor number for } sgTS \text{ tumors}}{\text{Tumor number for } sgInert \text{ tumors}}$$

761 The relative tumor number is a metric that reflects the probability of tumor initiation. If the
762 tumor suppressor genes normally constrain tumor initiation, inactivation of the gene will increase
763 the relative tumor number to be larger than 1.

764 Similarly, we normalized the observed tumor burden for sg*TS* tumors in *KT;H11*^{LSL-Cas9}
765 mice by dividing it by that of sg*TS* tumors. The relative tumor burden is calculated as the ratio of
766 the tumor burden for each sg*TS* relative to sg*Inert*:

767 Tumor burden = $\frac{\sum \text{neoplastic cell number in } KT; H11^{\text{LSL-Cas9}} \text{ mice}}{\sum \text{neoplastic cell number in } KT \text{ mice}}$ for each sg*TS*

768 Relative tumor burden = $\frac{\text{Tumor burden for sg} TS \text{ tumors}}{\text{Tumor burden for sg} Inert \text{ tumors}}$

769 The relative tumor burden is determined mostly by the largest tumors. For instance, the
770 top 1% of tumor cells accounts for over 50% of total tumor burden in *KT;H11*^{LSL-Cas9} mice at 11
771 weeks. Both *TS* inactivation that leads to faster overall growth, rare but exceptionally large
772 tumors and tumor initiation rate will result in an increase in relative tumor burden
773 (**Supplementary Fig. S4**).

774

775 **Bootstrapping the tumors**

776 In the calculation of confidence intervals and *P*-values, we needed to generate
777 distributions of the statistic considering both variation of tumor sizes across mice and within the
778 same mice. We adopted a two-step bootstrap resampling process. We first bootstrap resampled
779 mice to generate a pseudogroup of mice and then within each group of resampled mice, we
780 bootstrap resampled all observed tumors carrying each sgID.

781

782 **Calculation of confidence intervals and *P*-values for size metrics**

783 We have four size metrics that describe the overall growth (relative log-normal mean,
784 relative percentiles) and the heavy tailedness (relative Hill's estimator and relative steepness) of
785 the tumor size distribution. For each of these metrics, we bootstrapped tumors 10,000 times and

786 calculate 10,000 values of each statistic for these bootstrap resampling. The 95% confidence
787 interval is calculated as the 2.5th percentile and the 97.5th percentile of these bootstrapped results,
788 while the *P*-value is calculated the proportion of bootstrapped results that are not in the same
789 direction as the observed score compared with the baseline of 1.

790

791 **Calculation of *P*-values for tumor burden and tumor number**

792 We bootstrap tumors in both the *KT;H11^{LSL-Cas9}* and *KT* mice and calculate the relative
793 tumor burden and relative tumor number from these bootstrapped mice. The process was
794 repeated 10⁶ times. The 95% confidence interval is calculated as the 2.5th percentile and the
795 97.5th percentile of these bootstrapped results, while the *P*-value is calculated as the proportion
796 of bootstrapped values that are not in the same direction as the observed score compared with the
797 baseline of 1.

798

799 **Robustness to tumor burden differences**

800 To investigate whether overall tumor burden has an impact on genotype-specific tumor
801 initiation and growth, we calculated summary statistics for tumor initiation and tumor size
802 distribution on groups of mice with different overall tumor burden. Specifically, we divided the
803 47 *KT;H11^{LSL-Cas9}* mice with Lenti-sgTS102/Cre-initiated tumors at the 15-week time point into
804 three groups based on the total tumor burden in each mouse, namely the low tumor burden group
805 (16 mice), the medium tumor burden group (16 mice), and the high tumor burden group (15
806 mice). We performed calculations separately for each group for four metrics (95th percentile
807 tumor size, log-normal mean, tumor burden, and tumor number) and evaluated whether these
808 metrics show any correlation with tumor burden.

809

810 **Quantification of sex differences**

811 For each statistic, we use the ratio to quantify the differences between female mice and
812 male mice. The ratio is calculated as,

813
$$\text{Ratio} = \frac{X_{\text{Female}}}{X_{\text{Male}}}$$

814 Where X_{Male} and X_{Female} are the statistics quantified in male and female mice,
815 respectively. When calculating the P -values, we respectively bootstrapped tumors in male and
816 female mice and calculated the proportion of times that the bootstrapped results are not in the
817 same direction as the observed score compared with the baseline of 1.

818

819 **Empirical estimation of true positive rates**

820 We estimated the power (true positive rate) for each of the three experiments, (1) Lenti-
821 sgTS102/Cre; 15-week experiment, (2) Lenti-sgTS85/Cre; 15-week experiment, and (3) Lenti-
822 sgTS85/Cre; 26-week experiment. Understanding the true positive rate is important for
823 understanding the probability of identifying functional tumor suppressor genes. Since we do not
824 have a list for genuine functional tumor suppressor genes, we used each sgRNA that generated a
825 significant tumor suppressor effect (with nominal $P < 0.05$) as a proxy for true tumor suppressor
826 effects.

827 For each experiment, whenever we detected a significant effect for an sgRNA, we
828 queried whether the other sgRNA targeting that same gene also generated a significant tumor
829 suppressive effect. If the other sgRNA shows significant tumor suppressor effect, then the test is
830 counted as TRUE (T). If the second sgRNA fails to show a significant tumor suppressor effect,
831 then the test is FALSE (F). Across all sgRNA (including sgRNA#1 and sgRNA#2 for each

832 gene), we tallied the number of TRUE and FALSE discoveries. We used additive smoothing by
833 adding a pseudocount of 0.5 to both T and F counts to avoid the zero-probability problem in
834 some cases. Therefore, the estimated false negative rate for a gene targeted with a single sgRNA
835 would be:

836

$$p = \frac{F + 0.5}{(T + 0.5) + (F + 0.5)}$$

837 The estimated true positive rate in our experiment is the probability of failing to identify
838 a functional tumor suppressor gene with both of two sgRNAs. Thus, this is:

839 $\text{False negative rate} = p^2$

840 $\text{True positive rate} = 1 - \text{False negative rate} = 1 - p^2$

841 We performed this calculation separately for four metrics: 95th percentile, log-normal
842 mean, tumor burden, and tumor number. We did not estimate the true positive rate for Hill's
843 estimator because the number of positive findings was too few for robust estimations.

844

845 ***In vitro* analysis of sgRNA efficiency**

846 To analyze the relative cutting efficiencies of the sgRNAs, we measured the insertion and
847 deletion (indel) rates at the target sites in *Rosa26*^{LSL-Tomato}; *H1*^{LSL-Cas9} MEFs that were generated
848 from E12.5 embryos. These MEFs tested negative for mycoplasma contamination using the
849 MycoAlert mycoplasma detection kit (Lonza, cat# LT07-418). 10⁵ MEFs were transduced
850 individually with each Lenti-sgTS/Cre vector and cultured for 1 week followed by FACS-based
851 isolation of Tomato-positive transduced cells. Genomic DNA was extracted from sorted cells
852 using the QIAamp DNA Micro Kit (Qiagen 56304) and subjected to PCR-based target
853 enrichment. Two rounds of PCR were performed with Q5 Master Mix (NEB #M0494L). The
854 first round amplified each of the 97 sgRNA targeted regions (see **Supplementary Table S2** for

855 target-enrichment primer sequences). The second round added unique dual indexed Illumina
856 sequencing adaptors to the amplicons.

857 These libraries were sequenced on an Illumina NextSeq 500 in the 2x150 base-pair
858 paired-ended configuration (Admera Health Biopharma Services). The resulting reads were
859 demultiplexed based on their sample indexes. CRISPRessoPooled was used to quantify on-target
860 indel mutations (78). Briefly, pooled reads were initially demultiplexed into files according to
861 their specific sgRNA and aligned to the reference sequence to identify indel mutations.
862 Substitution events were ignored and all indels that occurred within 10 nucleotides of the
863 predicted target site (3 nucleotides upstream from the NGG PAM) were counted as on-target
864 indel mutations. Indel percent mutated was calculated as the number of reads with an on-target
865 indel divided by the total number of reads.

866

867 **Histology and immunohistochemistry (IHC)**

868 Lung lobes were inflated with PBS/4% paraformaldehyde and fixed for 24 hours, stored
869 in 70% ethanol, and paraffin-embedded and sectioned. 4 μm thick sections were used for
870 Hematoxylin and Eosin (H&E) staining and immunohistochemistry.

871 Primary antibodies used for IHC were anti-STAG2 (1:500, LifeSpan Cat# LS-B11284,
872 RRID:AB_2725802), anti-NKX2.1 (1: 250, Abcam Cat# ab76013, RRID:AB_1310784), anti-
873 Phospho-RPA2 (1:400, Abcam Cat# ab87277, RRID:AB_1952482), anti-Phospho-Histone
874 H2A.X (1:400, Cell Signaling Technology Cat# 9718, RRID:AB_2118009) and anti-Phospho-
875 ERK1/2 (1:400, Cell Signaling Technology Cat# 4370, RRID:AB_2315112). IHC was
876 performed using Avidin/Biotin Blocking Kit (Vector Laboratories, SP-2001), Avidin-Biotin
877 Complex kit (Vector Laboratories, PK-4001) and DAB Peroxidase Substrate Kit (Vector

878 Laboratories, SK-4100) following the standard protocols. Human lung adenocarcinoma tissue
879 microarrays were purchased from US Biomax (HLugA120PG01, BC041115e, LC1261, LC706a,
880 NSC155 and NSC157).

881

882 **Whole Genome Sequencing and quantitative RT-PCR**

883 For whole genome sequencing and qRT-PCR based gene expression analysis, samples
884 were generated from Lenti-Cre initiated tumors from three *KT* and three *KT;Stag2^{flox/flox}* mice (a
885 subset of samples from **Fig. 3G**). Briefly, neoplastic cells were isolated from pooled tumors
886 within two lung lobes of each mouse by FACS for Tomato^{positive} Lineage (CD45/CD31/F4-
887 80/Ter119)^{negative} cells (79). 60,000-100,000 neoplastic cells were collected from each mouse.
888 Genomic DNA and total RNA were purified using Qiagen AllPrep DNA/RNA Micro Kit (Cat#
889 80284). Genomic DNA was processed with Nextera Flex for karyotyping by low-pass (0.1x
890 coverage) whole genome sequencing. Log₂ ratio of reads mapping to each genomic locus versus
891 the average number of reads mapping to all other comparable loci was plotted.

892 For qRT-PCR total RNA was reverse-transcribed using Reliance Select cDNA Synthesis
893 Kit with oligo(dT) primers (BioRad Cat# 12012802). Quantitative PCR was performed with
894 PowerUp SYBR Green Master Mix (Thermo Fisher Scientific Cat# A25776) on an Applied
895 Biosystems QuantStudio 3 Real-Time PCR System. PCR primers were:
896 *Fos*: 5'-TACTACCATTCCCCAGCCGA-3' and 5'-GCTGTCACCGTGCGGGATAAA-3';
897 *Klf2*: 5'-GAGCCTATCTTGCCTCGCTT-3' and 5'-TTGTTTAGGTCTCATCCGTG-3';
898 *Ifnl3*: 5'-GTGCAGTTCCCACCTCATCT-3' and 5'-TGGGAGTGAATGTGGCTCAG-3';
899 *Ifnb1*: 5'-GTCCTCAACTGCTCTCCACT-3' and 5'-CATCCAGGCGTAGCTGTTGTA-3';
900 *Mxl*: 5'-ACGGTGCAGACATACCAGAA-3' and 5'-CTGTCTCCCTCTGATACGGT-3';

901 *Ifi44*: 5'-ATGGCAGCAAGAAAAGTGC-3' and 5'-AAACTTCTGCACACTCGCCT-3';
902 *Irf1*: 5'-CCAGAGATTGACAGGCCCTCG-3' and 5'-TGCACAAGGAATGGCCTGAA-3';
903 *Gapdh*: 5'-TGTGAACGGATTGGCCGTA-3' and 5'-ACTGTGCCGTTGAATTGCC-3';
904 *Actb*: 5'-GGCTCCTAGCACCATGAAGA-3' and 5'-GTGTAAAACGCAGCTCAGTAACA-3'.
905

906 Power analyses

907 Power analyses were used to evaluate the ability of the Tuba-seq platform to identify
908 functional tumor suppressors across a variety of experimental scenarios. The likelihood of
909 detecting a tumor suppressor depends on the strength of its effect, the number of mice assayed,
910 and the number of guides in the viral pool. We explored how these parameters influence
911 statistical power to detect genes affecting tumor growth and initiation through a pair of non-
912 parametric nested resampling approaches.

913 For each simulation that focused on tumor growth, a pseudo-cohort of mice ($n = 5, 10,$
914 $20, 50, 100, 200$) was sampled with replacement from the cohort of $47\text{ }KT;H11^{LSL-Cas9}$ mice
915 analyzed 15 weeks after tumor initiation, and statistical significance was assessed by bootstrap
916 resampling of tumors from the pseudo-cohort. For a given viral titer, a larger number of
917 multiplexed vectors results in fewer tumors with each sgRNA and a resulting loss of power due
918 to less thorough sampling of the underlying distribution of tumor sizes. To model this effect, the
919 number of tumors sampled from each mouse was scaled by the ratio of the number of sgIDs in
920 the underlying data to the simulated number of sgIDs ($n = 10, 20, 50, 100, 200, 500$). To capture
921 differences in power due to effect size, we performed analyses for representative strong,
922 moderate, and weak tumor suppressor-targeting sgRNAs (sg*Nf1*#1, sg*Rb1*#1, and sg*Dot1l*#1,
923 respectively). 500 simulations were performed for each gene, with a minimum of 16,000

924 bootstrap samplings per simulation. In each bootstrap, the size of tumor at the 95th percentile
925 with the focal genotype was compared to the size of tumor with sg*Inerts* at the 95th percentile,
926 and significance in each simulation was assessed by bootstrapped *P*-value <0.05 (two-tailed test,
927 Bonferroni-corrected for the simulated number of pooled sgRNAs).

928 Effects on tumor initiation are inferred through changes in the representation of tumor
929 genotypes in *KT;H11^{LSL-Cas9}* mice relative to the original proportions of the sgRNAs in the
930 lentiviral vector pool. As a result, identifying genes that influence tumor initiation requires
931 comparison of *KT;H11^{LSL-Cas9}* mice to *KT* mice, where the relative abundance of genotypes
932 reflects the make-up of the viral pool. For each simulation, we therefore sampled a cohort of both
933 *KT;H11^{LSL-Cas9}* and *KT* mice ($n = 5, 10, 20, 50, 100, 200$). For simplicity, we maintained the
934 approximate 4:1 ratio of *KT;H11^{LSL-Cas9}*:*KT* used in this study, while ensuring that there was
935 more than 1 *KT* mouse per cohort (e.g. for 50 total mice we sampled 40 *KT;H11^{LSL-Cas9}* and 10
936 *KT* mice). Analogous to the tumor size simulations, we model the effect of the number of pooled
937 sgRNAs by scaling the number of tumors sampled from each mouse by the ratio of the number
938 of sgIDs in the underlying data to the simulated number of sgIDs ($n = 10, 20, 50, 100, 200, 500$);
939 the resulting dataset was then bootstrapped to assess significance. To capture differences in
940 power due to effect size, analyses were performed for representative strong, moderate, and weak
941 suppressors of tumor initiation (sg*Pten*#2, sg*Kdm6a*#2, and sg*Ncoa6*#1, respectively). 500
942 simulations were performed for each gene, with a minimum of 16,000 bootstrap samplings per
943 simulation. In each bootstrap, the relative tumor number (ratio of number of tumors with focal
944 genotype to number of sg*Inert* tumors) in *KT;H11^{LSL-Cas9}* mice was compared to the relative
945 tumor number in *KT* mice, and significance in each simulation was assessed by bootstrapped *P*-
946 value <0.05 (two-tailed test, Bonferroni-corrected for the simulated number of pooled sgRNAs).

947

948 **DepMap data and filtering**

949 Cancer cell line dependency data (DepMap Public 19Q4) and mutation data (CCLE) were
950 acquired from the Broad Institute DepMap Portal (RRID:SCR_017655)(59). Lung
951 adenocarcinoma cell lines were identified by their Project Achilles identification code. For each
952 gene of interest, the cell lines that contained damaging mutations within the gene were identified
953 and flagged. Damaging mutations were defined as mutations that likely caused loss of gene
954 function. Subsequently, dependency scores for each gene of interest were exported from both the
955 complete dataset of lung adenocarcinoma cell lines and dataset of cell lines that contains no
956 damaging mutation in the gene of interest. Finally, the distribution of dependency scores across
957 each gene of interest was plotted using GraphPad Prism 8.

958

959 **REFERENCES**

- 960 1. Hanahan D, Weinberg RA. Hallmarks of cancer: the next generation. *Cell*
961 **2011**;144(5):646-74 doi 10.1016/j.cell.2011.02.013.
- 962 2. Consortium APG. AACR Project GENIE: Powering Precision Medicine through an
963 International Consortium. *Cancer Discov* **2017**;7(8):818-31 doi 10.1158/2159-8290.CD-
964 17-0151.
- 965 3. Consortium ITP-CAoWG. Pan-cancer analysis of whole genomes. *Nature*
966 **2020**;578(7793):82-93 doi 10.1038/s41586-020-1969-6.
- 967 4. Cancer Genome Atlas Research N. Comprehensive molecular profiling of lung
968 adenocarcinoma. *Nature* **2014**;511(7511):543-50 doi 10.1038/nature13385.

- 969 5. Zehir A, Benayed R, Shah RH, Syed A, Middha S, Kim HR, *et al.* Mutational landscape
970 of metastatic cancer revealed from prospective clinical sequencing of 10,000 patients. Nat
971 Med **2017**;23(6):703-13 doi 10.1038/nm.4333.
- 972 6. Jamal-Hanjani M, Wilson GA, McGranahan N, Birkbak NJ, Watkins TBK, Veeriah S, *et*
973 *al.* Tracking the Evolution of Non-Small-Cell Lung Cancer. N Engl J Med
974 **2017**;376(22):2109-21 doi 10.1056/NEJMoa1616288.
- 975 7. Cancer Genome Atlas Research N, Weinstein JN, Collisson EA, Mills GB, Shaw KR,
976 Ozenberger BA, *et al.* The Cancer Genome Pan-Cancer analysis project. Nat Genet
977 **2013**;45(10):1113-20 doi 10.1038/ng.2764.
- 978 8. Bailey MH, Tokheim C, Porta-Pardo E, Sengupta S, Bertrand D, Weerasringhe A, *et al.*
979 Comprehensive Characterization of Cancer Driver Genes and Mutations. Cell
980 **2018**;173(2):371-85 e18 doi 10.1016/j.cell.2018.02.060.
- 981 9. Lawrence MS, Stojanov P, Polak P, Kryukov GV, Cibulskis K, Sivachenko A, *et al.*
982 Mutational heterogeneity in cancer and the search for new cancer-associated genes. Nature
983 **2013**;499(7457):214-8 doi 10.1038/nature12213.
- 984 10. Greaves M, Maley CC. Clonal evolution in cancer. Nature **2012**;481(7381):306-13 doi
985 10.1038/nature10762.
- 986 11. Stratton MR, Campbell PJ, Futreal PA. The cancer genome. Nature **2009**;458(7239):719-
987 24 doi 10.1038/nature07943.
- 988 12. Winters IP, Murray CW, Winslow MM. Towards quantitative and multiplexed *in vivo*
989 functional cancer genomics. Nat Rev Genet **2018**;19(12):741-55 doi 10.1038/s41576-018-
990 0053-7.

- 991 13. Zahir N, Sun R, Gallahan D, Gatenby RA, Curtis C. Characterizing the ecological and
992 evolutionary dynamics of cancer. *Nat Genet* **2020**;52(8):759-67 doi 10.1038/s41588-020-
993 0668-4.
- 994 14. Ben-David U, Beroukhim R, Golub TR. Genomic evolution of cancer models: perils and
995 opportunities. *Nat Rev Cancer* **2019**;19(2):97-109 doi 10.1038/s41568-018-0095-3.
- 996 15. Graham TA, Sottoriva A. Measuring cancer evolution from the genome. *J Pathol*
997 **2017**;241(2):183-91 doi 10.1002/path.4821.
- 998 16. McGranahan N, Swanton C. Biological and therapeutic impact of intratumor heterogeneity
999 in cancer evolution. *Cancer Cell* **2015**;27(1):15-26 doi 10.1016/j.ccr.2014.12.001.
- 1000 17. Garraway LA, Lander ES. Lessons from the cancer genome. *Cell* **2013**;153(1):17-37 doi
1001 10.1016/j.cell.2013.03.002.
- 1002 18. Howard TP, Vazquez F, Tsherniak A, Hong AL, Rinne M, Aguirre AJ, *et al.* Functional
1003 Genomic Characterization of Cancer Genomes. *Cold Spring Harb Symp Quant Biol*
1004 **2016**;81:237-46 doi 10.1101/sqb.2016.81.031070.
- 1005 19. Friedman AA, Letai A, Fisher DE, Flaherty KT. Precision medicine for cancer with next-
1006 generation functional diagnostics. *Nat Rev Cancer* **2015**;15(12):747-56 doi
1007 10.1038/nrc4015.
- 1008 20. Weber J, Braun CJ, Saur D, Rad R. In vivo functional screening for systems-level
1009 integrative cancer genomics. *Nat Rev Cancer* **2020**;20(10):573-93 doi 10.1038/s41568-
1010 020-0275-9.
- 1011 21. Kersten K, de Visser KE, van Miltenburg MH, Jonkers J. Genetically engineered mouse
1012 models in oncology research and cancer medicine. *EMBO Mol Med* **2017**;9(2):137-53 doi
1013 10.15252/emmm.201606857.

- 1014 22. Sanchez-Rivera FJ, Papagiannakopoulos T, Romero R, Tammela T, Bauer MR, Bhutkar
1015 A, *et al.* Rapid modelling of cooperating genetic events in cancer through somatic genome
1016 editing. *Nature* **2014**;516(7531):428-31 doi 10.1038/nature13906.
- 1017 23. Annunziato S, Kas SM, Nethe M, Yucel H, Del Bravo J, Pritchard C, *et al.* Modeling
1018 invasive lobular breast carcinoma by CRISPR/Cas9-mediated somatic genome editing of
1019 the mammary gland. *Genes Dev* **2016**;30(12):1470-80 doi 10.1101/gad.279190.116.
- 1020 24. Chiou SH, Winters IP, Wang J, Naranjo S, Dudgeon C, Tamburini FB, *et al.* Pancreatic
1021 cancer modeling using retrograde viral vector delivery and in vivo CRISPR/Cas9-mediated
1022 somatic genome editing. *Genes Dev* **2015**;29(14):1576-85 doi 10.1101/gad.264861.115.
- 1023 25. Xue W, Chen S, Yin H, Tammela T, Papagiannakopoulos T, Joshi NS, *et al.* CRISPR-
1024 mediated direct mutation of cancer genes in the mouse liver. *Nature* **2014**;514(7522):380-
1025 4 doi 10.1038/nature13589.
- 1026 26. Rogers ZN, McFarland CD, Winters IP, Naranjo S, Chuang CH, Petrov D, *et al.* A
1027 quantitative and multiplexed approach to uncover the fitness landscape of tumor
1028 suppression in vivo. *Nat Methods* **2017**;14(7):737-42 doi 10.1038/nmeth.4297.
- 1029 27. Rogers ZN, McFarland CD, Winters IP, Seoane JA, Brady JJ, Yoon S, *et al.* Mapping the
1030 in vivo fitness landscape of lung adenocarcinoma tumor suppression in mice. *Nat Genet*
1031 **2018**;50(4):483-6 doi 10.1038/s41588-018-0083-2.
- 1032 28. Winters IP, Chiou SH, Paulk NK, McFarland CD, Lalgudi PV, Ma RK, *et al.* Multiplexed
1033 in vivo homology-directed repair and tumor barcoding enables parallel quantification of
1034 Kras variant oncogenicity. *Nat Commun* **2017**;8(1):2053 doi 10.1038/s41467-017-01519-
1035 y.

- 1036 29. Kumar RD, Searleman AC, Swamidass SJ, Griffith OL, Bose R. Statistically identifying
1037 tumor suppressors and oncogenes from pan-cancer genome-sequencing data.
1038 *Bioinformatics* **2015**;31(22):3561-8 doi 10.1093/bioinformatics/btv430.
- 1039 30. The Gene Ontology C. The Gene Ontology Resource: 20 years and still GOing strong.
1040 *Nucleic Acids Res* **2019**;47(D1):D330-D8 doi 10.1093/nar/gky1055.
- 1041 31. Iwanaga K, Yang Y, Raso MG, Ma L, Hanna AE, Thilaganathan N, *et al.* Pten inactivation
1042 accelerates oncogenic K-ras-initiated tumorigenesis in a mouse model of lung cancer.
1043 *Cancer Res* **2008**;68(4):1119-27 doi 10.1158/0008-5472.CAN-07-3117.
- 1044 32. Ji H, Ramsey MR, Hayes DN, Fan C, McNamara K, Kozlowski P, *et al.* LKB1 modulates
1045 lung cancer differentiation and metastasis. *Nature* **2007**;448(7155):807-10 doi
1046 10.1038/nature06030.
- 1047 33. Walter DM, Venancio OS, Buza EL, Tobias JW, Deshpande C, Gudiel AA, *et al.*
1048 Systematic In Vivo Inactivation of Chromatin-Regulating Enzymes Identifies Setd2 as a
1049 Potent Tumor Suppressor in Lung Adenocarcinoma. *Cancer Res* **2017**;77(7):1719-29 doi
1050 10.1158/0008-5472.CAN-16-2159.
- 1051 34. Wang X, Min S, Liu H, Wu N, Liu X, Wang T, *et al.* Nf1 loss promotes Kras-driven lung
1052 adenocarcinoma and results in Psat1-mediated glutamate dependence. *EMBO Mol Med*
1053 **2019**;11(6) doi 10.15252/emmm.201809856.
- 1054 35. Werner M, Purta E, Kaminska KH, Cymerman IA, Campbell DA, Mittra B, *et al.* 2'-O-
1055 ribose methylation of cap2 in human: function and evolution in a horizontally mobile
1056 family. *Nucleic Acids Res* **2011**;39(11):4756-68 doi 10.1093/nar/gkr038.

- 1057 36. Koo BK, Spit M, Jordens I, Low TY, Stange DE, van de Wetering M, *et al*. Tumour
1058 suppressor RNF43 is a stem-cell E3 ligase that induces endocytosis of Wnt receptors.
1059 *Nature* **2012**;488(7413):665-9 doi 10.1038/nature11308.
- 1060 37. Jiang X, Hao HX, Gowney JD, Woolfenden S, Bottiglio C, Ng N, *et al*. Inactivating
1061 mutations of RNF43 confer Wnt dependency in pancreatic ductal adenocarcinoma. *Proc
1062 Natl Acad Sci U S A* **2013**;110(31):12649-54 doi 10.1073/pnas.1307218110.
- 1063 38. Koo BK, van Es JH, van den Born M, Clevers H. Porcupine inhibitor suppresses paracrine
1064 Wnt-driven growth of Rnf43;Znrf3-mutant neoplasia. *Proc Natl Acad Sci U S A*
1065 **2015**;112(24):7548-50 doi 10.1073/pnas.1508113112.
- 1066 39. Balbas-Martinez C, Sagrera A, Carrillo-de-Santa-Pau E, Earl J, Marquez M, Vazquez M,
1067 *et al*. Recurrent inactivation of STAG2 in bladder cancer is not associated with aneuploidy.
1068 *Nat Genet* **2013**;45(12):1464-9 doi 10.1038/ng.2799.
- 1069 40. Romero-Perez L, Surdez D, Brunet E, Delattre O, Grunewald TGP. STAG Mutations in
1070 Cancer. *Trends Cancer* **2019**;5(8):506-20 doi 10.1016/j.trecan.2019.07.001.
- 1071 41. Solomon DA, Kim JS, Bondaruk J, Shariat SF, Wang ZF, Elkahloun AG, *et al*. Frequent
1072 truncating mutations of STAG2 in bladder cancer. *Nat Genet* **2013**;45(12):1428-30 doi
1073 10.1038/ng.2800.
- 1074 42. Viny AD, Bowman RL, Liu Y, Lavallee VP, Eisman SE, Xiao W, *et al*. Cohesin Members
1075 Stag1 and Stag2 Display Distinct Roles in Chromatin Accessibility and Topological
1076 Control of HSC Self-Renewal and Differentiation. *Cell Stem Cell* **2019**;25(5):682-96 e8
1077 doi 10.1016/j.stem.2019.08.003.

- 1078 43. Kleyman M, Kabeche L, Compton DA. STAG2 promotes error correction in mitosis by
1079 regulating kinetochore-microtubule attachments. *J Cell Sci* **2014**;127(Pt 19):4225-33 doi
1080 10.1242/jcs.151613.
- 1081 44. Solomon DA, Kim T, Diaz-Martinez LA, Fair J, Elkahloun AG, Harris BT, *et al.* Mutational
1082 inactivation of STAG2 causes aneuploidy in human cancer. *Science*
1083 **2011**;333(6045):1039-43 doi 10.1126/science.1203619.
- 1084 45. Kong X, Ball AR, Jr., Pham HX, Zeng W, Chen HY, Schmiesing JA, *et al.* Distinct
1085 functions of human cohesin-SA1 and cohesin-SA2 in double-strand break repair. *Mol Cell*
1086 *Biol* **2014**;34(4):685-98 doi 10.1128/MCB.01503-13.
- 1087 46. Mondal G, Stevers M, Goode B, Ashworth A, Solomon DA. A requirement for STAG2 in
1088 replication fork progression creates a targetable synthetic lethality in cohesin-mutant
1089 cancers. *Nat Commun* **2019**;10(1):1686 doi 10.1038/s41467-019-09659-z.
- 1090 47. Shen CH, Kim SH, Trousil S, Frederick DT, Piris A, Yuan P, *et al.* Loss of cohesin complex
1091 components STAG2 or STAG3 confers resistance to BRAF inhibition in melanoma. *Nat*
1092 *Med* **2016**;22(9):1056-61 doi 10.1038/nm.4155.
- 1093 48. Ding S, Diep J, Feng N, Ren L, Li B, Ooi YS, *et al.* STAG2 deficiency induces interferon
1094 responses via cGAS-STING pathway and restricts virus infection. *Nat Commun*
1095 **2018**;9(1):1485 doi 10.1038/s41467-018-03782-z.
- 1096 49. Inoki K, Li Y, Zhu T, Wu J, Guan KL. TSC2 is phosphorylated and inhibited by Akt and
1097 suppresses mTOR signalling. *Nat Cell Biol* **2002**;4(9):648-57 doi 10.1038/ncb839.
- 1098 50. Shilatifard A. The COMPASS family of histone H3K4 methylases: mechanisms of
1099 regulation in development and disease pathogenesis. *Annu Rev Biochem* **2012**;81:65-95
1100 doi 10.1146/annurev-biochem-051710-134100.

- 1101 51. Wu Q, Tian Y, Zhang J, Tong X, Huang H, Li S, *et al.* In vivo CRISPR screening unveils
1102 histone demethylase UTX as an important epigenetic regulator in lung tumorigenesis. Proc
1103 Natl Acad Sci U S A **2018**;115(17):E3978-E86 doi 10.1073/pnas.1716589115.
- 1104 52. Hill BM. A Simple General Approach to Inference About the Tail of a Distribution. The
1105 Annals of Statistics **1975**;3(5):1163-74.
- 1106 53. Jackson EL, Olive KP, Tuveson DA, Bronson R, Crowley D, Brown M, *et al.* The
1107 differential effects of mutant p53 alleles on advanced murine lung cancer. Cancer Res
1108 **2005**;65(22):10280-8 doi 10.1158/0008-5472.CAN-05-2193.
- 1109 54. Feldser DM, Kostova KK, Winslow MM, Taylor SE, Cashman C, Whittaker CA, *et al.*
1110 Stage-specific sensitivity to p53 restoration during lung cancer progression. Nature
1111 **2010**;468(7323):572-5 doi 10.1038/nature09535.
- 1112 55. Johnson L, Mercer K, Greenbaum D, Bronson RT, Crowley D, Tuveson DA, *et al.* Somatic
1113 activation of the K-ras oncogene causes early onset lung cancer in mice. Nature
1114 **2001**;410(6832):1111-6 doi 10.1038/35074129.
- 1115 56. Gao Q, Steine EJ, Barrasa MI, Hockemeyer D, Pawlak M, Fu D, *et al.* Deletion of the de
1116 novo DNA methyltransferase Dnmt3a promotes lung tumor progression. Proc Natl Acad
1117 Sci U S A **2011**;108(44):18061-6 doi 10.1073/pnas.1114946108.
- 1118 57. Schuster K, Venkateswaran N, Rabellino A, Girard L, Pena-Llopis S, Scaglioni PP.
1119 Nullifying the CDKN2AB locus promotes mutant K-ras lung tumorigenesis. Mol Cancer
1120 Res **2014**;12(6):912-23 doi 10.1158/1541-7786.MCR-13-0620-T.
- 1121 58. Andricovich J, Perkail S, Kai Y, Casasanta N, Peng W, Tzatsos A. Loss of KDM6A
1122 Activates Super-Enhancers to Induce Gender-Specific Squamous-like Pancreatic Cancer

- 1123 and Confers Sensitivity to BET Inhibitors. *Cancer Cell* **2018**;33(3):512-26 e8 doi
1124 10.1101/j.ccell.2018.02.003.
- 1125 59. Tsherniak A, Vazquez F, Montgomery PG, Weir BA, Kryukov G, Cowley GS, *et al.*
1126 Defining a Cancer Dependency Map. *Cell* **2017**;170(3):564-76 e16 doi
1127 10.1101/j.cell.2017.06.010.
- 1128 60. Lawrence MS, Stojanov P, Mermel CH, Robinson JT, Garraway LA, Golub TR, *et al.*
1129 Discovery and saturation analysis of cancer genes across 21 tumour types. *Nature*
1130 **2014**;505(7484):495-501 doi 10.1038/nature12912.
- 1131 61. Rheinbay E, Nielsen MM, Abascal F, Wala JA, Shapira O, Tiao G, *et al.* Analyses of non-
1132 coding somatic drivers in 2,658 cancer whole genomes. *Nature* **2020**;578(7793):102-11
1133 doi 10.1038/s41586-020-1965-x.
- 1134 62. Alexandrov LB, Kim J, Haradhvala NJ, Huang MN, Tian Ng AW, Wu Y, *et al.* The
1135 repertoire of mutational signatures in human cancer. *Nature* **2020**;578(7793):94-101 doi
1136 10.1038/s41586-020-1943-3.
- 1137 63. Curry NL, Mino-Kenudson M, Oliver TG, Yilmaz OH, Yilmaz VO, Moon JY, *et al.* Pten-
1138 null tumors cohabiting the same lung display differential AKT activation and sensitivity to
1139 dietary restriction. *Cancer Discov* **2013**;3(8):908-21 doi 10.1158/2159-8290.CD-12-0507.
- 1140 64. Yanagi S, Kishimoto H, Kawahara K, Sasaki T, Sasaki M, Nishio M, *et al.* Pten controls
1141 lung morphogenesis, bronchioalveolar stem cells, and onset of lung adenocarcinomas in
1142 mice. *J Clin Invest* **2007**;117(10):2929-40 doi 10.1172/JCI31854.
- 1143 65. Ciriello G, Cerami E, Sander C, Schultz N. Mutual exclusivity analysis identifies
1144 oncogenic network modules. *Genome Res* **2012**;22(2):398-406 doi
1145 10.1101/gr.125567.111.

- 1146 66. van de Haar J, Canisius S, Yu MK, Voest EE, Wessels LFA, Ideker T. Identifying Epistasis
1147 in Cancer Genomes: A Delicate Affair. *Cell* **2019**;177(6):1375-83 doi
1148 10.1016/j.cell.2019.05.005.
- 1149 67. Li C, Lin WY, Rizvi H, Cai H, McFarland CD, Rogers ZN, *et al.* Quantitative in vivo
1150 analyses reveal a complex pharmacogenomic landscape in lung adenocarcinoma. *bioRxiv*
1151 **2020**. Preprint: <https://www.biorxiv.org/content/10.1101/2020.01.28.923912v1>
- 1152 68. Foggetti G, Li C, Cai H, Hellyer JA, Lin WY, Ayeni D, *et al.* Genetic determinants of
1153 EGFR-Driven Lung Cancer Growth and Therapeutic Response In Vivo. *Cancer Discovery*
1154 **In press.**
- 1155 69. Ellrott K, Bailey MH, Saksena G, Covington KR, Kandoth C, Stewart C, *et al.* Scalable
1156 Open Science Approach for Mutation Calling of Tumor Exomes Using Multiple Genomic
1157 Pipelines. *Cell Syst* **2018**;6(3):271-81 e7 doi 10.1016/j.cels.2018.03.002.
- 1158 70. McGranahan N, Favero F, de Bruin EC, Birkbak NJ, Szallasi Z, Swanton C. Clonal status
1159 of actionable driver events and the timing of mutational processes in cancer evolution. *Sci
1160 Transl Med* **2015**;7(283):283ra54 doi 10.1126/scitranslmed.aaa1408.
- 1161 71. Tate JG, Bamford S, Jubb HC, Sondka Z, Beare DM, Bindal N, *et al.* COSMIC: the
1162 Catalogue Of Somatic Mutations In Cancer. *Nucleic Acids Res* **2019**;47(D1):D941-D7 doi
1163 10.1093/nar/gky1015.
- 1164 72. Hough SH, Kancleris K, Brody L, Humphryes-Kirilov N, Wolanski J, Dunaway K, *et al.*
1165 Guide Picker is a comprehensive design tool for visualizing and selecting guides for
1166 CRISPR experiments. *BMC Bioinformatics* **2017**;18(1):167 doi 10.1186/s12859-017-
1167 1581-4.

- 1168 73. Doench JG, Fusi N, Sullender M, Hegde M, Vaimberg EW, Donovan KF, *et al.* Optimized
1169 sgRNA design to maximize activity and minimize off-target effects of CRISPR-Cas9. *Nat*
1170 *Biotechnol* **2016**;34(2):184-91 doi 10.1038/nbt.3437.
- 1171 74. Hsu PD, Scott DA, Weinstein JA, Ran FA, Konermann S, Agarwala V, *et al.* DNA
1172 targeting specificity of RNA-guided Cas9 nucleases. *Nat Biotechnol* **2013**;31(9):827-32
1173 doi 10.1038/nbt.2647.
- 1174 75. Bae S, Kweon J, Kim HS, Kim JS. Microhomology-based choice of Cas9 nuclease target
1175 sites. *Nat Methods* **2014**;11(7):705-6 doi 10.1038/nmeth.3015.
- 1176 76. Madisen L, Zwingman TA, Sunkin SM, Oh SW, Zariwala HA, Gu H, *et al.* A robust and
1177 high-throughput Cre reporting and characterization system for the whole mouse brain. *Nat*
1178 *Neurosci* **2010**;13(1):133-40 doi 10.1038/nn.2467.
- 1179 77. Jackson EL, Willis N, Mercer K, Bronson RT, Crowley D, Montoya R, *et al.* Analysis of
1180 lung tumor initiation and progression using conditional expression of oncogenic K-ras.
1181 *Genes & Development* **2001**;15(24):3243-8 doi DOI 10.1101/gad.943001.
- 1182 78. Clement K, Rees H, Canver MC, Gehrke JM, Farouni R, Hsu JY, *et al.* CRISPResso2
1183 provides accurate and rapid genome editing sequence analysis. *Nat Biotechnol*
1184 **2019**;37(3):224-6 doi 10.1038/s41587-019-0032-3.
- 1185 79. Chuang CH, Greenside PG, Rogers ZN, Brady JJ, Yang D, Ma RK, *et al.* Molecular
1186 definition of a metastatic lung cancer state reveals a targetable CD109-Janus kinase-Stat
1187 axis. *Nat Med* **2017**;23(3):291-300 doi 10.1038/nm.4285.
- 1188

1189 **FIGURE LEGENDS**

1190 **Figure 1. An *in vivo* screen for tumor suppressor genes in autochthonous oncogenic *Kras*-
1191 driven lung tumors.**

1192 (A) Candidate tumor suppressor genes were chosen based on multiple criteria including their
1193 frequency and known/predicted biological functions. The plot shows the mutation frequencies of
1194 these 48 genes across pan-cancer and in lung adenocarcinoma (data from TCGA). Color denotes
1195 lung adenocarcinoma driver consensus score derived from multiple prediction tools. Several genes
1196 that are mutated at high frequency in lung adenocarcinoma or pan-cancer are labeled.

1197 (B) Features of the mutations in each gene are consistent with tumor suppressor function. Green's
1198 contagion is a measure of mutational hotspots, which characterize oncogenes. Larger values
1199 indicate that mutations are enriched in particular residues of the protein. This measure of
1200 overdispersion is normalized to not scale with sample size and to be zero when mutations are
1201 randomly scattered across the transcript. Average fraction of protein lost by mutation combines
1202 the nonsense/frameshift mutation rate and location of the mutations in each gene [(percent of
1203 protein transcript altering mutations that are nonsense or frameshift)*(Average fraction of protein
1204 lost by nonsense or frameshift mutations)].

1205 (C) Schematic of tumor initiation with our pool of 102 barcoded Lenti-sgRNA/Cre vectors (Lenti-
1206 sgTS102/Cre). Each gene is targeted with two sgRNAs, except p53 which is targeted by three
1207 sgRNAs. 5 Inert sgRNAs are either non-targeting (NT) or have an active targeting but inert
1208 sgRNAs (which target *Neo*^R in the *R26*^{LSL-Tomato} allele). Barcoded Lentiviral vectors contain an
1209 sgRNA, Cre, and a 2-component barcode that includes an sgRNA identifier (sgID) and random
1210 barcode (BC). This allows inactivation of multiple target genes in parallel followed by
1211 quantification of the number of neoplastic cells by high-throughput sgID-BC sequencing. Mouse

1212 genotype, mouse number, and titer of lentiviral vectors are indicated. Tuba-seq was performed on
1213 each tumor-bearing lung 15 weeks after initiation, followed by analyses to quantify the indicated
1214 metrics. ifu, infectious units.

1215 (D) Fluorescence images of lungs from representative mice at 15 weeks after tumor initiation.
1216 Lung lobes are outlined with a dashed white line. Scale bars = 2 mm.

1217 (E) Pearson correlation coefficient (r) and P -value (two-tailed) suggest strong correlation between
1218 neoplastic cell number (an indicator of tumor burden) and lung weight. Each dot represents a
1219 mouse. When taking into account that tumors were initiated in $KT;H11^{LSL-Cas9}$ mice with 3-fold
1220 less Lenti-sgTS102/Cre vectors, the total neoplastic cell number is ~10-fold greater in $KT;H11^{LSL-}$
1221 $Cas9$ mice than in KT mice.

1222 (F) Volcano plot of the impact of inactivating each putative tumor suppressor gene on relative
1223 tumor burden. Each dot represents an sgRNA. Inert sgRNAs are in gray. Tumor suppressor genes
1224 are colored pink when both sgRNAs trigger moderate but significant increase and green when one
1225 sgRNA triggers >4 fold increase and the other triggers moderate but significant increase. Data is
1226 aggregated from 47 $KT;H11^{LSL-Cas9}$ and 12 KT mice.

1227

1228 **Figure 2. *In vivo* lung tumor growth is suppressed by diverse tumor suppressor genes.**

1229 (A) The 95th percentile tumor size (normalized to tumors with sgInerts) for each putative tumor
1230 suppressor targeting sgRNA in $KT;H11^{LSL-Cas9}$ mice. Error bars indicate 95% confidence intervals.
1231 95% confidence intervals and P -values were calculated by bootstrap. sgRNAs that significantly
1232 increase or decrease tumor size are colored as indicated. sgInerts are in gray and the dotted line
1233 indicates no effect. Genes are ordered based on the average of the 95th percentile tumor sizes from

1234 all sgRNAs targeting that gene, individual sgRNAs targeting each gene were ranked by effect for
1235 clarity. Pearson correlation coefficient (r) and P -value (two tailed) suggest that sgRNAs targeting
1236 the same putative tumor suppressor elicit consistent and similar changes in size at 95th percentile.

1237 (B) Tumor sizes at the indicated percentiles for the top 17 tumor suppressor genes (relative to the
1238 average of sg*Inert*-containing tumors) in *KT;H11^{LSL-Cas9}* mice. Error bars indicate 95% confidence
1239 intervals. Dotted line indicates no effect. Percentiles that are significantly different from the
1240 average of sg*Inerts* are in color. Data for all genes is shown in **Supplementary Fig. S5B**. Pearson
1241 correlation coefficient (r) and P -value (two-tailed) for all sgRNA across all indicated percentiles
1242 are shown.

1243 (C) The log-normal mean tumor size (normalized to tumors with sg*Inerts*) for each putative tumor
1244 suppressor targeting sgRNA in *KT;H11^{LSL-Cas9}* mice. Error bars indicate 95% confidence intervals.
1245 95% confidence intervals and P -values were calculated by bootstrap. sgRNAs that significantly
1246 increase or decrease tumor size are colored as indicated. sg*Inerts* are in gray and the dotted line
1247 indicates no effect. Genes and sgRNAs are ordered as in **Fig. 2A**. The high Pearson's correlation
1248 coefficient suggests that sgRNAs targeting the same putative tumor suppressor elicit consistent
1249 and similar changes in log-normal mean tumor size.

1250 All plots represent aggregated data from 47 *KT;H11^{LSL-Cas9}*.

1251

1252 **Figure 3. Stag2, inactivation of which increases tumor burden and reduces survival, is**
1253 **frequently lowly expressed in human lung adenocarcinoma.**

1254 (A) Cre/lox-mediated Stag2 inactivation promotes *Kras*^{G12D}-driven lung tumor growth. Lung
1255 tumors were initiated in indicated genotypes of mice with Lenti-Cre and allowed to grow for 15
1256 weeks.

1257 (B) Representative fluorescence images of lung lobes from the indicated genotypes and genders
1258 of mice are shown. Scale bars = 5 mm.

1259 (C) Lenti-Cre initiated tumors in indicated *KT;Stag2*^{fl/fl} mice lack Stag2 protein expression.
1260 Scale bar = 50 mm.

1261 (D) Lung weight from indicated genotypes of mice 15 weeks after tumor initiation with Lenti-Cre.
1262 Each dot represents a mouse and the bar is the mean. *P*-values were calculated by Student's t-test.

1263 (E) Inactivation of Stag2 increases lung tumor growth *in vivo*. Representative histology is shown.
1264 Genotype and gender are indicated. Scale bars = 1 mm.

1265 (F) Quantification of tumor area (%) (tumor area/total lung area x 100) on H&E-stained sections
1266 of mouse lungs 15 weeks after tumor initiation. Each dot represents a mouse and the bar is the
1267 mean. *P*-values were calculated by Student's t-test.

1268 (G) Survival curve of mice with KrasG12D-driven lung tumors that are either Stag2 wild-type
1269 (*KT;Stag2*^{w/w} female and *KT;Stag2*^{w/y} male mice), Stag2 heterozygous (*KT;Stag2*^{f/w}), or Stag2
1270 deficient (*KT;Stag2*^{f/f} female and *KT;Stag2*^{f/y} male mice). Mouse number, *P*-value and
1271 median survival (in days) are indicated. *P*-values were calculated by comparing each cohort to the
1272 Stag2 wild-type cohort (Mantel-Haenszel test).

1273 (H) Representative STAG2 IHC on human lung adenocarcinomas expressing high (positive) or
1274 low (low and negative) STAG2 protein. Scale bars = 100 μ m.

1275 (I) Quantification of STAG2 expression in 479 human lung adenocarcinomas. Data are grouped
1276 by tumor grade (left, with lower grade indicating well-differentiated tumors and higher grade
1277 indicating poorly differentiated tumors) or by tumor stage (right, classified by TNM staging
1278 system). A higher percentage of *Stag2*^{low/neg} tumors are poorly differentiated (left) and more
1279 advanced (right) tumors.

1280

1281 **Figure 4. Exaggeration of tumor phenotypes and emergence of more functional tumor**
1282 **suppressors over time.**

1283 (A) Schematic of tumor initiation with a pool of 85 barcoded Lenti-sgRNA/Cre vectors (Lenti-
1284 sgTS85/Cre) which excludes 8 tumor suppressor genes (in gray and crossed out) from the Lenti-
1285 sgTS102/Cre pool whose losses collectively account for ~60% of total tumor burden. Each gene is
1286 targeted with two sgRNAs. Mouse genotype, mouse number, and titer of lentiviral vectors
1287 delivered to each mouse are indicated. Tuba-seq was performed on each tumor-bearing lung at the
1288 indicated time after tumor initiation.

1289 (B) Volcano plot of the impact of inactivating each putative tumor suppressor gene on relative
1290 tumor burden. Each dot represents an sgRNA. Genes for which both sgRNA increase tumor burden
1291 are colored.

1292 (C,D) The impact of inactivating each gene on the size of the 95th percentile tumor (C) and log-
1293 normal mean (D) at 15 weeks (Lenti-sgTS102/Cre 15 weeks) and 26 weeks (Lenti-sgTS85/Cre 26
1294 weeks) after tumor initiation is shown. Each dot represents an sgRNA. Statistics are calculated
1295 from aggregating all tumors from 40 *KT;H11*^{LSL-Cas9} (26 weeks) and 47 *KT;H11*^{LSL-Cas9} (15 weeks)
1296 mice.

1297 (E) Heatmap of the tumor suppressive effects of six genes that emerge as suppressors of tumor
1298 growth at the later timepoint. Colors indicate the impact of inactivating each gene on tumor size
1299 at 15 weeks (Lenti-sgTS102/Cre 15 weeks and Lenti-sgTS85/Cre 15 weeks) and 26 weeks (Lenti-
1300 sgTS85/Cre 26 weeks) after tumor initiation, and sizes of the tiles indicate statistical significance
1301 levels.

1302 (F) Sizes of tumors at the indicated percentiles for each Lenti-sgRNA/Cre vector relative to that
1303 of sgInert-targeted tumors in *KT;H11^{LSL-Cas9}* mice. Error bars indicate 95% confidence intervals.
1304 Percentiles that are significantly different from the average of sgInerts are in color. Data for all
1305 genes is shown in **Supplementary Fig. S9B**.

1306

1307 **Figure 5. Tumor initiation is inhibited by diverse tumor suppressor genes independent of**
1308 **their effects on tumor growth.**

1309 (A) Inactivation of many tumor suppressor genes increases tumor number, highlighting pathways
1310 that normally constrain the earliest steps of carcinogenesis. The effect of each sgRNA on tumor
1311 number 15 weeks after tumor initiation with Lenti-sgTS102/Cre in *KT;H11^{LSL-Cas9}* mice is shown.
1312 Error bars indicate 95% confidence intervals. 95% confidence intervals and *P*-values were
1313 calculated by bootstrap. sgRNAs that significantly increase or decrease tumor number are colored
1314 as indicated. sgInerts are in gray and the dotted line indicates no effect. Genes and sgRNAs are
1315 ordered as in **Fig. 2A**.

1316 (B) Genotype specific effects on growth (represented by the size of the tumor at the 95th percentile)
1317 and tumor number can be independent aspects of tumor suppression.

1318 (C,D) Mutation frequency of members of the COMPASS complex in human lung adenocarcinoma.
1319 Data are shown as the number of patients with mutations in one or more of the COMPASS complex
1320 subunits/total patient number from GENIE/IMPACT (C) as well as TCGA and TRACERx (D).
1321 Data from GENIE/IMPACT are based on panel sequencing and therefore does not include data on
1322 NCOA6. Data from TRACERx are from multi-region sequencing where we report the number of
1323 tumors that had any of these four genes mutated in one or more regions.

1324 (E) The effect of each sgRNA on tumor number 26 weeks after tumor initiation with Lenti-
1325 sgTS85/Cre in *KT;H11^{LSL-Cas9}* mice is shown. Error bars indicate 95% confidence intervals. 95%
1326 confidence intervals and *P*-values were calculated by bootstrap. sgRNAs that significantly increase
1327 or decrease tumor number are colored as indicated. sgInerts are in gray and the dotted line indicates
1328 no effect. Genes and sgRNAs are ordered as in (A).

1329 (F) Effects of tumor suppressor gene inactivation on tumor number are highly reproducible. The
1330 impact of inactivating each gene on tumor number at 15 weeks (Lenti-sgTS102/Cre 15 weeks) and
1331 26 weeks (Lenti-sgTS85/Cre 26 weeks) after tumor initiation is shown. Each dot represents an
1332 sgRNA. Statistics are calculated from aggregating all tumors from all mice in each group in each
1333 experiment. Pearson correlation coefficient (*r*) shows correlation.

1334

1335 **Figure 6. Loss of *p53*, *Cdkn2a* and *Dnmt3a* result in rare yet exceptionally large tumors.**

1336 (A) Plot of tumor sizes for each indicated sgRNA in *KT;H11^{LSL-Cas9}* mice at 15 weeks. Each dot
1337 represents a tumor and the area of the dot scales with neoplastic cell number within the tumor. For
1338 better visualization, an equal number of tumors (n=1160) are shown for each sgRNA.

1339 (B) Volcano plot of the impact of inactivating each putative tumor suppressor gene on the
1340 distribution of tumor sizes (Hill's estimator compares tumors above the 95th percentile to those at
1341 the 95th percentile to quantify the relative size of tumors in the tail of the distribution). *P53*- and
1342 *Dnmt3a*-targeted tumors are heavy-tailed, suggesting that loss of these genes promoted the
1343 emergence of exceptionally large tumors. Each dot represents an sgRNA.

1344 (C) Plot of tumor sizes for each indicated sgRNA in *KT;H11^{LSL-Cas9}* mice at 26 weeks. Each dot
1345 indicates a tumor, and the area of the dot indicates neoplastic cell number within the tumor. Equal
1346 number of tumors (814 tumors randomly sampled) are shown for each sgRNA.

1347 (D) Volcano plot of the impact of inactivating each putative tumor suppressor gene on the
1348 developing of infrequent exceptionally large tumors (Hill's estimator). Each dot represents an
1349 sgRNA. Statistics are calculated from aggregating all tumors from 40 *KT;H11^{LSL-Cas9}* (26 weeks)
1350 mice.

1351 (E) Inactivation of *Dnmt3a* and *Cdkn2a* generate tumor size distributions with heavy tails.
1352 Probability density plots for tumor sizes show the profile of aggregated tumors with *sgInerts* as
1353 well as individual sgRNAs targeting either *Dnmt3a* or *Cdkn2a*. Data is aggregated from all tumors
1354 from 40 *KT;H11^{LSL-Cas9}* (26 weeks) mice.

1355

1356 **Figure 7. Tumor suppressors constrain tumorigenesis at different stages and to different**
1357 **levels.**

1358 (A) Radar plots of representative genes whose inactivation affects tumor size at the 95th percentile
1359 (relative to *sgInerts*, indicating increased overall growth), tumor number (relative to *sgInerts*,

1360 indicating increased tumor initiation) and Hill's estimator (relative to *sgInerts*, indicating increased
1361 rare large tumors). Tumor suppressors suppress different aspects of tumor development.

1362 (B) Heatmap summarizing the tumor size at the 95th percentile (relative to *sgInerts*), tumor number
1363 (relative to *sgInerts*) and Hill's estimator (relative to *sgInerts*) of the functional tumor suppressor
1364 genes. Color scale is indicated on the side. Bolded circles indicate bootstrap $P < 0.05$. Although
1365 the sizes of *Ubr5*-, *Tsc1*-, *Kdm6a*- and *Ncoa6*-deficient tumors are not significantly different from
1366 control tumors at 95th percentile, they are significantly greater across multiple percentiles at 26
1367 weeks, and thus they are also considered genes that suppress tumor growth.

1368 (C) Summary schematic of a tumor suppression map in lung adenocarcinoma based on our data.

Figure 1

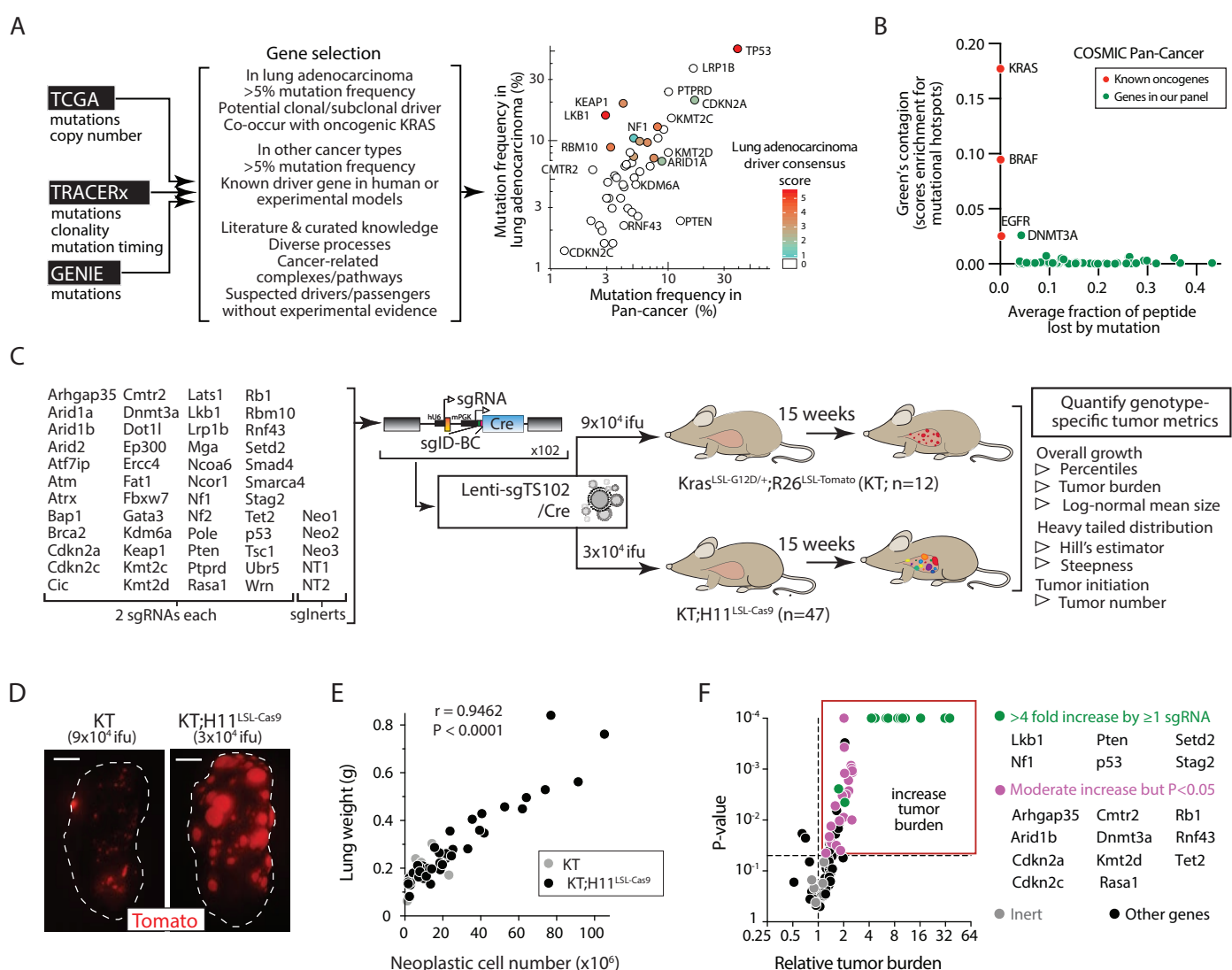


Figure 2

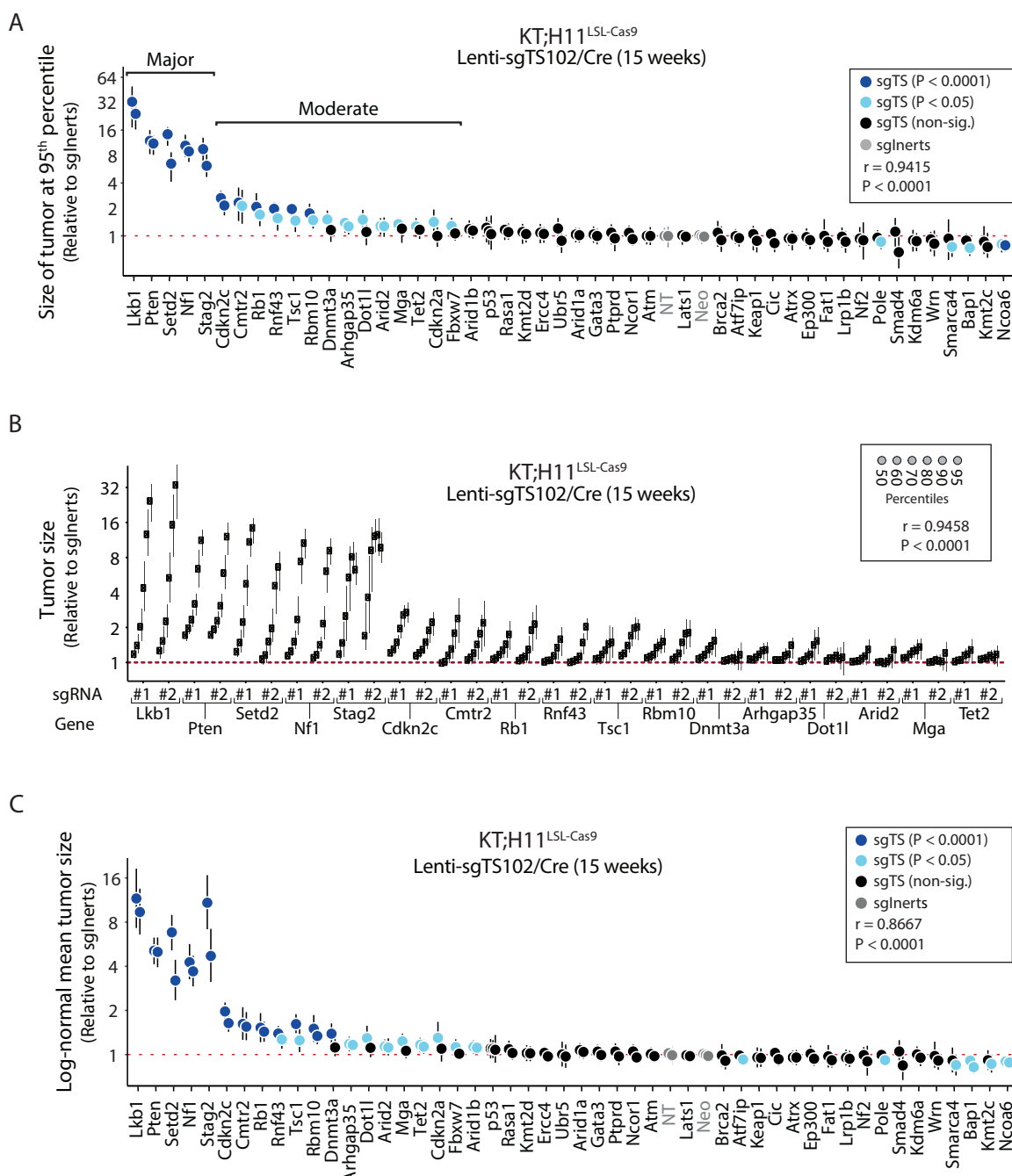


Figure 3

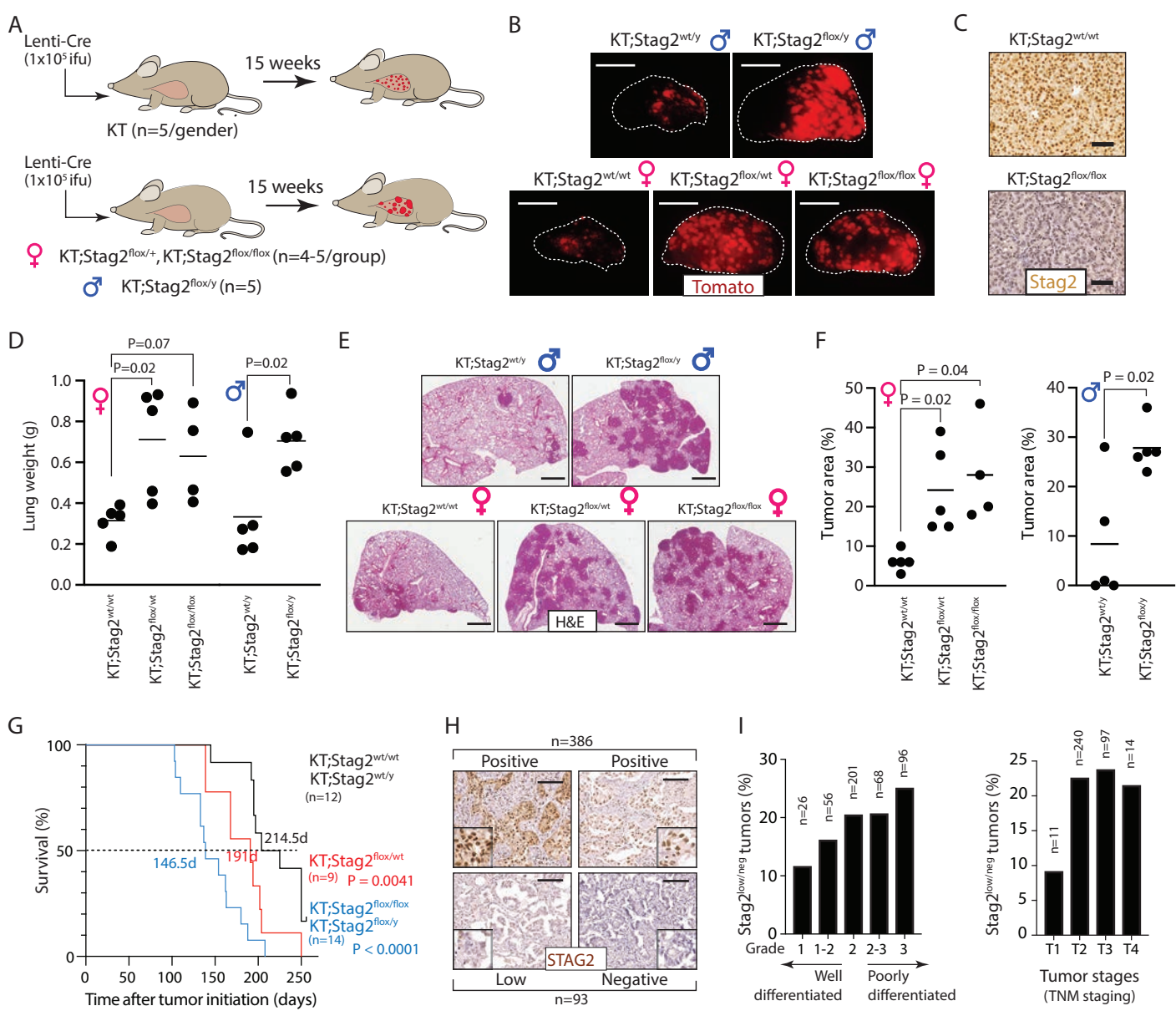


Figure 4

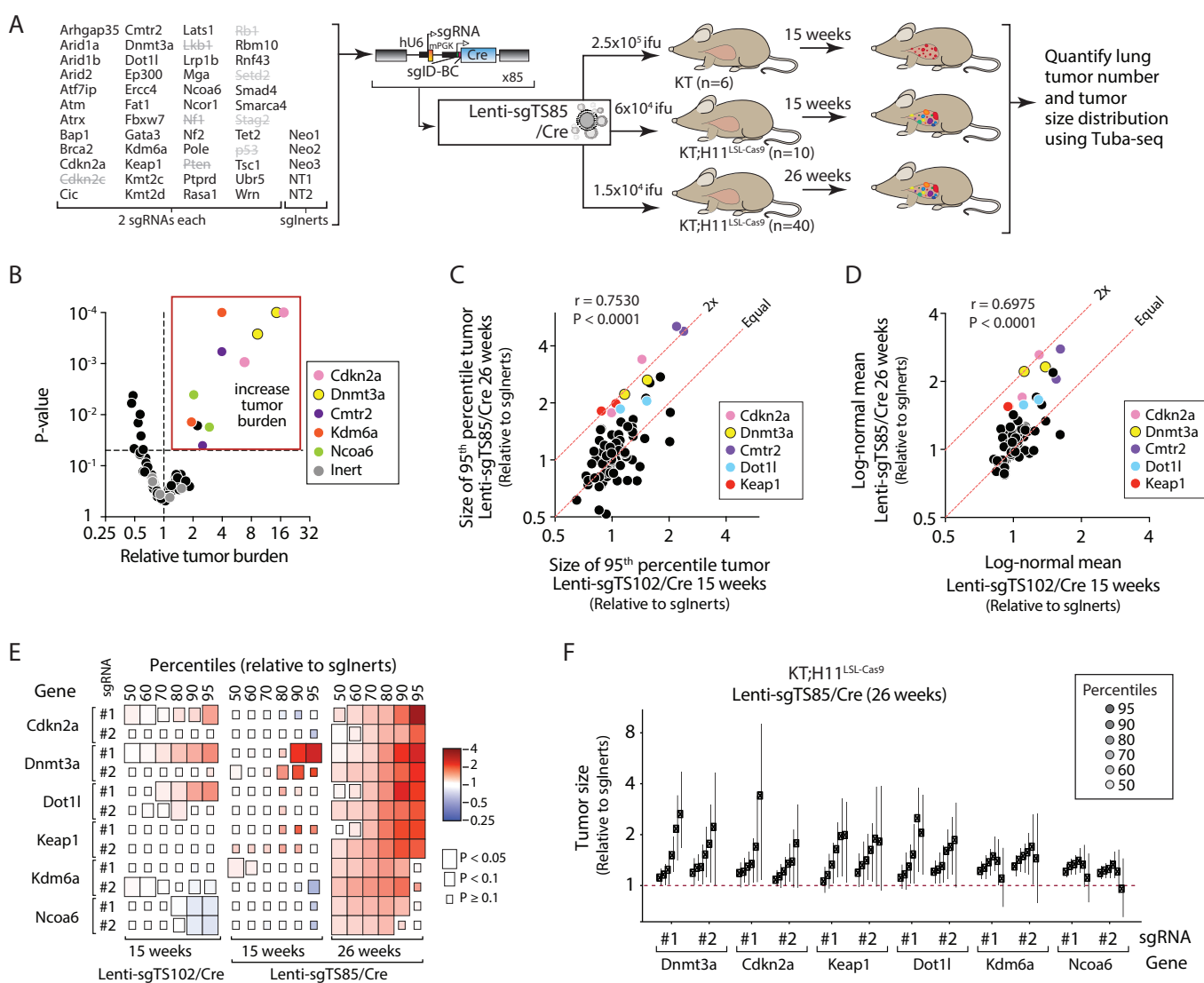


Figure 5

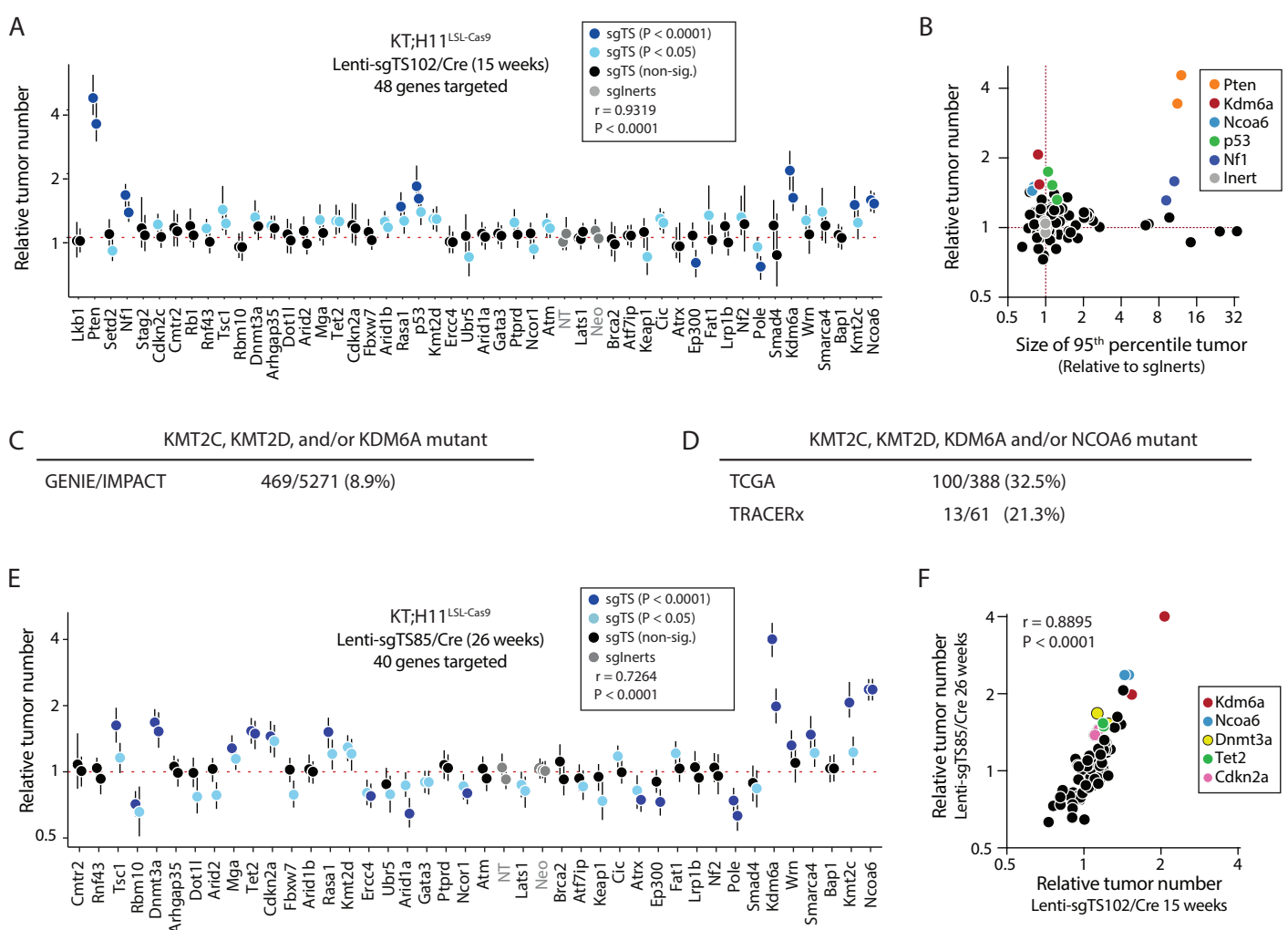


Figure 6

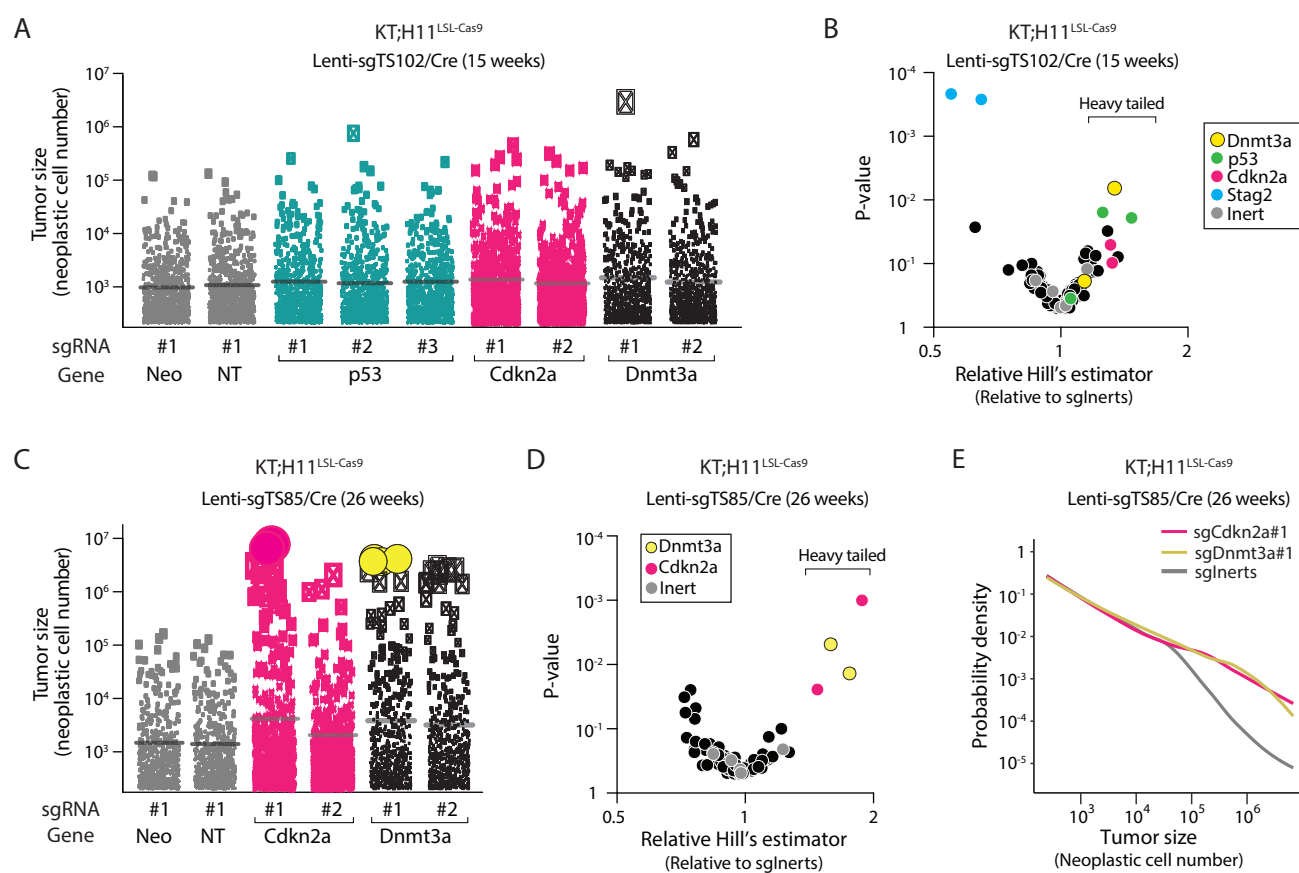
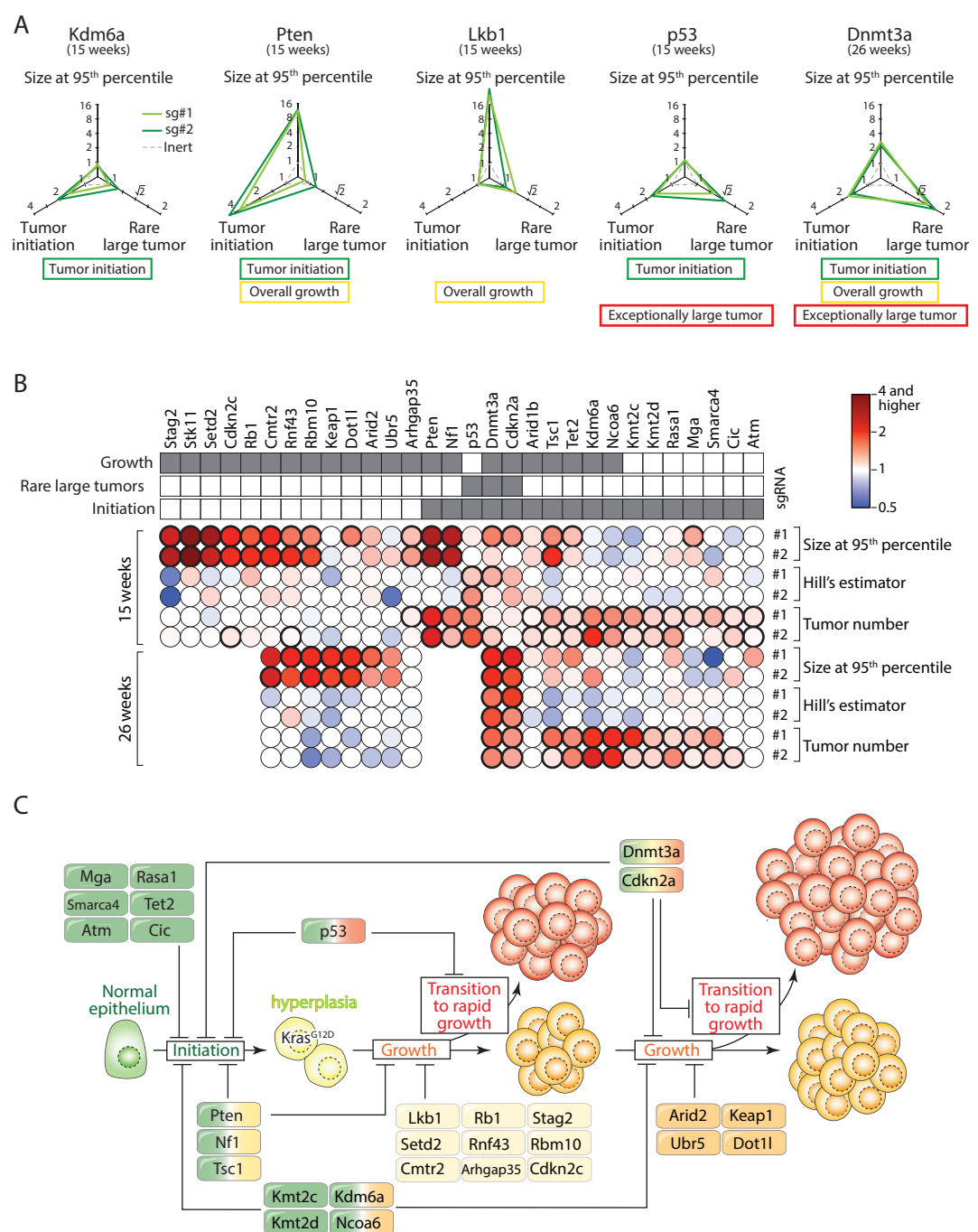


Figure 7



CANCER DISCOVERY

A functional taxonomy of tumor suppression in oncogenic KRAS-driven lung cancer

Hongchen Cai, Su Kit Chew, Chuan Li, et al.

Cancer Discov Published OnlineFirst February 19, 2021.

Updated version	Access the most recent version of this article at: doi: 10.1158/2159-8290.CD-20-1325
Supplementary Material	Access the most recent supplemental material at: http://cancerdiscovery.aacrjournals.org/content/suppl/2021/02/17/2159-8290.CD-20-1325.DC1
Author Manuscript	Author manuscripts have been peer reviewed and accepted for publication but have not yet been edited.

E-mail alerts	Sign up to receive free email-alerts related to this article or journal.
Reprints and Subscriptions	To order reprints of this article or to subscribe to the journal, contact the AACR Publications Department at pubs@aacr.org .
Permissions	To request permission to re-use all or part of this article, use this link http://cancerdiscovery.aacrjournals.org/content/early/2021/02/16/2159-8290.CD-20-1325 . Click on "Request Permissions" which will take you to the Copyright Clearance Center's (CCC) Rightslink site.